

obtained in the *Abca12*^{-/-} newborns after treatment.⁵ After our publication, Zuo et al⁶ also reported another *Abca12* knockout mouse, whose skin showed similar features to our model mice.

Previously, we demonstrated severe skin barrier defects in *Abca12*^{-/-} mice and suggested that "barrier insufficiency" plays an important role in HI phenotype expression.⁵ However, "the barrier insufficiency" theory fails to completely explain the pathomechanism of the HI phenotype. HI fetuses show a HI phenotype even *in utero*, where skin barrier protection against a dry environment is not required. In addition, the skin phenotype of HI long-term survivors maintained in a dry environment shows a dramatic improvement within several weeks after birth where they require a normal skin barrier function. Thus, we suspected that other unknown mechanisms are involved in HI and the formation HI survivors' skin phenotypes. To date there have been no reports which have compared the skin phenotypes in fatally affected HI neonates and survivors, and the exact mechanism of HI survivors' skin phenotype improvement has yet to be clarified. Thus, we have carefully analyzed the keratinization process of neonatal versus grafted HI model mice skin and primary versus subcultured *Abca12*^{-/-} keratinocytes instead of human HI neonatal and survivors' skin. Initially, we investigated the distribution and amounts/composition of lipids, and expression of differentiation-specific molecules in neonatal HI model mice skin. Then, we studied the alteration of them in grafted HI model mouse skin transplanted onto severe combined immunodeficient (SCID) mice. In addition, we performed keratinocyte culture experiments including immunostaining and Western blotting using primary/subcultured *Abca12*^{-/-} keratinocytes to confirm the results of the neonatal and grafted skin experiments. Further, we analyzed the whole gene expression profile of primary versus subcultured *Abca12*^{-/-} keratinocytes using cDNA microarray methods. Finally, we conducted therapeutic trials on primary-cultured *Abca12*^{-/-} keratinocytes and grafted HI model mice skin with retinoids.

Materials and Methods

Animals

All animal studies were reviewed and approved by the Animal Use and Care Committee of the Hokkaido University Graduate School of Medicine. C57BL/6 strain mice and SCID mice were purchased from Clea (Tokyo, Japan). All animals used for this study were maintained under pathogen-free conditions.

Antibodies

Rabbit polyclonal affinity purified anti-mouse *Abca12* antibody was raised in rabbits using a 14-amino acid sequence synthetic peptide (residues 2581 to 2594) derived from the mouse *Abca12* sequence (XM001002308) as the immunogen.⁵ The other primary antibodies were rabbit anti-profilaggrin/filaggrin antibody (COVANCE, Princeton, NJ), rabbit anti-involucrin antibody (M-116; Santa Cruz Biotechnology, Santa Cruz, CA), rabbit anti-desmo-

glein 1 antibody (H-290; Santa Cruz Biotechnology), rabbit anti-mouse loricrin antibody (AF62; COVANCE), rabbit anti-kallikrein 5 antibody (ab7283; Abcam, Cambridge, UK), rabbit anti-glucosylceramide/ceramide antibody (Glycobio-tech, Kukels, Germany), and mouse monoclonal anti- β actin antibody (Sigma Chemical Co., St. Louis, MO). Secondary antibodies used in the present study were as follows; Alexa Fluor 488-conjugated donkey anti-rabbit IgG (Invitrogen Corp., Carlsbad, CA), fluorescein isothiocyanate-conjugated goat anti-rabbit IgG (Jackson Immuno Research, West Grove, PA), horseradish peroxidase-conjugated goat anti-rabbit IgG or horseradish peroxidase-conjugated goat anti-mouse IgG (Invitrogen Corp.).

Generation of *Abca12*^{-/-} Mouse

The procedure for generating *Abca12*^{-/-} mice has been previously described.⁵ Briefly, we cloned mouse genomic DNA *Abca12* fragments from the mouse 129Sv/Ev genomic library (Bacpac Resources Center, Children's Hospital Oakland Research Institute, Oakland, CA). We subcloned a 10.6-kb fragment to make the targeting vector. We inserted the PGK/Neo cassette between 47 bp upstream of the exon 30 and 203 bp downstream of exon 30. We transfected the targeting vector by electroporation into 129Sv/Ev embryonic stem cells, then microinjected the correctly targeted embryonic stem cell line into blastocysts obtained from C57BL/6 mice to generate chimeric mice, which we then mated with C57BL/6 females. We crossed the heterozygotes with C57BL/6 over at least five generations, and then intercrossed them to generate the *Abca12*^{-/-} mice. Genotyping was performed by PCR as described previously.⁵

Establishment of *Abca12*^{-/-} Mice Keratinocyte Culture

Skin samples from *Abca12*^{-/-} and wild-type mice were processed for primary keratinocyte culture, and cells were grown according to standard procedures in CnT-57 medium (Cellntec Advanced Cell Systems, Bern, Switzerland). For differentiation induction, culture medium was switched from CnT-57 medium to CnT-02 medium (Cellntec Advanced Cell Systems) and, 24 hours later, the calcium concentration was changed to 1.2 mmol/L. 48 hours later, we performed extractions of total RNA and protein from cultured cells. We established primary-cultured keratinocytes from two *Abca12*^{-/-} mice and two wild-type mice.

Skin Grafting

In total, ten *Abca12*^{-/-} and three wild-type neonates were sacrificed by anesthesia with ether inhalation, and their dorsal skin excised and transplanted onto SCID mice (Clea). Those skin grafts were fully adapted within 2 weeks after grafting. At 3 weeks after transplantation, the skin grafts were harvested for further analysis.

Extraction of Total RNA and Real-Time Reverse Transcriptase PCR Analysis

We separated the epidermis from whole skin samples of wild and *Abca12*^{-/-} mice by 1 mol/L NaCl in sterile water at 4°C for 2 hours. We isolated total RNA from the epidermis using the Quick Gene RNA Tissue Kit SII (Fujifilm Corp, Tokyo, Japan). We also isolated total RNA from keratinocytes cultured from wild-type and *Abca12*^{-/-} skin using the RNeasy mini kit (Qiagen Corp, Tokyo, Japan). RNA concentration was measured spectrophotometrically and samples were stored at -80°C until use for reverse transcriptase PCR. We reverse-transcribed RNA using Superscript II (Invitrogen Corp.) following the manufacturer's instructions. Complementary DNA samples were analyzed by ABI prism 7000 sequence detection system (Applied Biosystems, Foster City, CA). Primers and probes specific for differentiation-specific protein genes including loricrin, kallikrein 5, transglutaminase 1, involucrin, filaggrin, and control house keeping genes, glyceraldehyde-3-phosphate dehydrogenase (GAPDH), and β -actin, were obtained from Taqman Gene Expression Assay (Applied Biosystems) (Probe ID: Mm01962650_s1, Mm01203811_a1, Mm00498375_a1, Mm00515219_s1, Mm01716522_m1, Mm99999915_g1, and Mm00607939_s1). Differences between the mean CT values of loricrin, kallikrein 5, transglutaminase 1, involucrin, filaggrin and those of GAPDH or β -actin were calculated as: $\Delta\text{CT}_{Abca12^{-/-}} \text{ mice} = \text{CT}_{\text{loricrin}}$ (or other keratinization markers) - CT_{GAPDH} (or other house keeping genes) and those of ΔCT for the *Abca12*^{+/+} as $\Delta\text{CT}_{\text{calibrator}} = \text{CT}_{\text{loricrin}}$ (or other keratinization markers) - CT_{GAPDH} (or other house keeping genes).

We could obtain the similar results from GAPDH and β -actin standard, thus we described the results of GAPDH standard in the present study. Final results for *Abca12*^{-/-} mouse samples/wild-type mouse samples (%) were determined by $2^{-\Delta\Delta\text{CT}_{Abca12^{-/-}} \text{ sample} - \Delta\text{CT}_{\text{calibrator}}}$. We measured mRNA levels five times for each clones. Using similar methods, we quantitatively analyzed these differentiation-specific mRNA expression levels in the primary/subcultured keratinocytes from *Abca12*^{-/-} and wild-type mice.

Western Blotting

We separated the epidermis from whole skin samples of wild and *Abca12*^{-/-} mice by 1 mol/L NaCl in sterile water at 4°C for 2 hours. For Western blotting, we used epidermal homogenates and proteins extracted from cultured keratinocytes prepared with radioimmunoprecipitation assay (RIPA) buffer comprising 50 mmol/L Tris-HCl, pH7.5, 150 mmol/L NaCl, 1% Nonidet P-40, 0.5% deoxycholate, 0.1% SDS, and Roche protease cocktail tablet (Roche, Basel, Switzerland). Protein concentrations were measured using Micro BCA protein assay kit (Thermo Scientific, Rockford, IL). Protein concentration of the samples for western blotting was from 1 to 2 $\mu\text{g}/\mu\text{l}$. The 20 μg protein loading per single lane was separated by a 5 to 20% gradient gel SDS-polyacrylamide gel and transferred to polyvinylidene difluoride membranes. Membrane blocking and incubation with anti-

bodies were performed in Tris-buffered saline with 2% non-fat dry milk. Signals were revealed with chemiluminescence reagents and photographed by LAS-1000 mini (Fujifilm Corp, Tokyo, Japan). We also confirmed the loading protein dose by β -actin antibody staining as internal protein control. For analysis of filaggrin solubility and processing, epidermal lysates were prepared with RIPA buffer. Samples of precipitated proteins in the RIPA buffer were solubilized again in 8 mol/L urea before boiling in reducing SDS loading buffer.

Light Microscopy and Immunofluorescence Analysis

For light microscopy, we harvested the newborn pups' skin and the grafted skin, and fixed them for 24 hours in 10% neutral buffered formalin, dehydrated them in graded ethanol, and embedded them in paraffin. We cut 4- μm sections and stained them with H&E. For immunohistochemistry, the tissue samples were embedded in optimal cutting temperature compound (Sakura Finetechnical Corp., Tokyo, Japan). Frozen tissue sections were cut at a thickness of 5 μm . The sections were blocked with 1% bovine serum albumin (BSA) in PBS for 30 minutes at room temperature, and incubated in primary antibody solution in blocking buffer for 30 minutes at 37°C. Fluorescent labeling was performed with secondary antibodies, followed by propidium iodide (Sigma Chemical Co.) for 5 minutes at room temperature to counterstain nuclei. The stained samples were observed under an Olympus Fluoview confocal laser-scanning microscope (Olympus, Tokyo, Japan).

In Situ Transglutaminase Activity

The procedure for *in situ* transglutaminase 1 activity assay has been previously described.^{7,8} In brief, unfixed cryosections of 5 μm were blocked with 100 mmol/L Tris-HCl pH7.4, 1% BSA for 30 minutes, and then incubated with 100 mmol/L Tris-HCl pH7.4, 5 mmol/L CaCl_2 , 12 $\mu\text{mol/L}$ monodansylcadaverine (Sigma) for 1 hour to detect transglutaminase 1 activity. For negative controls, EDTA was added to the monodansylcadaverine solution to a final concentration of 20 mmol/L. After stopping the transglutaminase 1 reaction with 10 mmol/L EDTA in PBS, sections were incubated with rabbit anti-dansyl antibody (Invitrogen Corp.) in 12% BSA/PBS for 3 hours. Sections were then incubated with fluorescein isothiocyanate-conjugated goat anti-rabbit antibody in 12% BSA/PBS for 30 minutes. Nuclei were counterstained by propidium iodide. The stained samples were observed under an Olympus Fluoview confocal laser-scanning microscope (Olympus).

Immunofluorescence Labeling of Cultured Cells

Immunofluorescence labeling of cultured cells was performed as previously described.⁵ Briefly, primary/subcultured keratinocytes were fixed in 4% paraformaldehyde for 15 minutes and permeabilized with 0.1% Triton X-100 for 15 minutes at room temperature. Keratinocytes were blocked with 1% BSA in PBS for 30 minutes at room temperature,

and incubated in primary antibody solution in blocking buffer for 30 minutes at 37°C and fluorescence labeling was performed with secondary antibodies, followed by propidium iodide for 5 minutes at room temperature to counterstain nuclei. The stained samples were observed under an Olympus Fluoview confocal laser-scanning microscope (Olympus).

Electron Microscopy

Neonatal skin samples and skin grafts were fixed in 5% glutaraldehyde solution, post fixed in 1% OsO₄, dehydrated, and embedded in Epon 812 (TAAB Laboratories, Berkshire, UK). All of the samples were ultra-thin sectioned at a thickness of 70 nm, and stained with uranyl acetate and lead citrate. Photographs were taken using a Hitachi H-7100 transmission electron microscope (Hitachi, Tokyo, Japan).

Lipid Analysis

Lipid analysis was performed as previously reported.⁹ Briefly, lipid analysis was done independently on three *Abca12*^{-/-} neonates, two wild-type as controls, and two mature *Abca12*^{-/-} skins 3 months after skin grafting and two mature wild-type skins 3 months after transplantation as control. We separated the epidermis from whole skin specimens of control and *Abca12*^{-/-} mice by incubation in sterile water at 60°C for 1 minute and homogenized in 0.8 ml of PBS. A total lipid component was extracted from tissue homogenates of epidermis according to conventional methods.⁹ Lipid analysis in epidermal lysates from neonates and grafted skin was performed by liquid chromatography, electrospray ionization mass spectrometry (LC-ESI-MS) using a HP 1100 liquid chromatography system (Agilent Technologies, Palo Alto, CA).

Measurement of Transepidermal Water Loss

Transepidermal water loss (TEWL) from the skin of neonatal mice and from skin grafted onto SCID mice was measured by evaporimeter (AS-VT100RS; Asahi Biomed Corp., Yokohama, Japan), as described previously.⁵ The AS-VT100RS utilizes the ventilated-chamber method for measuring TEWL. Its hygrometer measures the humidity of incoming air and of outgoing air that has passed over the test area of the skin, and TEWL is calculated from the difference. TEWL measurements were performed on the back of the neonates and the grafted skin onto the back of SCID mice.

Complementary DNA Microarray Analysis for the Gene Expression Profile

Total RNA isolated from primary/subcultured *Abca12*^{-/-} keratinocytes was extracted as described above. Total RNA concentration was calculated spectrophotometrically, and quality control of RNA was analyzed with an Agilent 2100 Bioanalyzer (Agilent Technologies, Tokyo, Japan). mRNA/cDNA hybrids were generated via T7oligo dT primers, fol-

lowed by addition of DNA polymerase and ligase (Filgen, Nagoya, Japan) to obtain double-stranded cDNA. The sample tagged with chemiluminescent substrate, Cy3 for the subcultured *Abca12*^{-/-} keratinocytes, or Cy5 for the primary-cultured *Abca12*^{-/-} keratinocytes, was hybridized on a microarray chip (Filgen Array mouse 32K, Filgen). We used a mixture of total RNAs from the two cultures for labeling reactions. Fluorescence images for Cy3 and Cy5 dye channels were obtained using a GenePix 4000B scanner (Axon Instruments, CA) and scan data images were analyzed using Microarray Data Analysis Tool version 3.0 software (Filgen).

Therapeutic Trial with Retinoids on Primary-Cultured *Abca12*^{-/-} Keratinocytes and Grafted Harlequin Ichthyosis Model Mice Skin

To test the efficacy of a therapeutic trial on primary-cultured *Abca12*^{-/-} keratinocytes, isotretinoin (purchased by Sigma Chemical Co., St. Louis, MO) was dissolved in dimethyl sulfoxide (DMSO). In addition, etretinate powder (a gift from Chugai Pharmaceuticals, Tokyo, Japan) was dissolved in sterile water.

Primary-cultured keratinocytes were grown in CnT-57 medium (Cellntec Advanced Cell Systems) and then switched into CnT-02 medium (Cellntec Advanced Cell Systems). Twenty-four hours later, the calcium concentration was changed to 1.2 mmol/L in CnT-02 medium with retinoids (10⁻⁶ mol/L isotretinoin or 10⁻⁶ mol/L etretinate) dissolved in DMSO or water. The final concentration of DMSO in medium was 0.01%. As control, keratinocytes were cultured in CnT-02 medium with 1.2 mmol/L calcium supplemented with 0.01% DMSO without retinoids. Forty-eight hours later, we extracted protein from keratinocytes.

In a therapeutic trial using grafted HI model mice skin, we dissolved several doses of isotretinoin in soy oil, and single doses (1, 10 mg/kg) of isotretinoin were administered orally into the grafted SCID mice 3 weeks after skin transplantation every day for 10 days.

Statistical Analysis

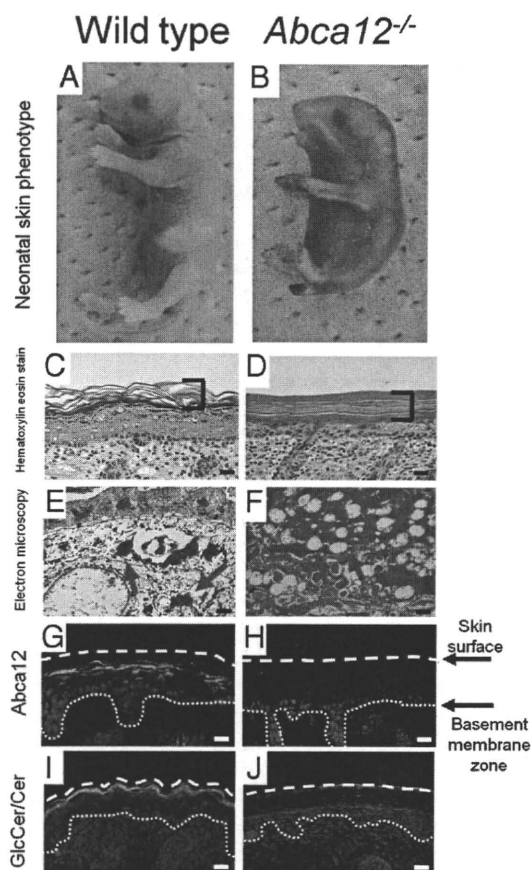
All statistical analyses were performed using student's *t*-tests with sample sizes indicated in the figure legends for each comparison that was made. *P* values of <0.05 were considered statistically significant.

Results

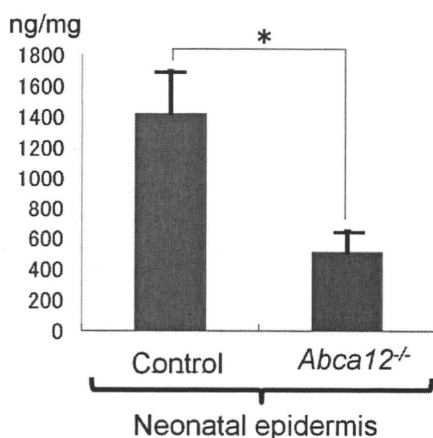
Abca12^{-/-} Neonatal Mouse Epidermis Exhibited Defective Lipid Distribution, Reduced Expression of Differentiation-Specific Proteins and Profilaggrin/Filaggrin Conversion Defects

As we previously reported,⁵ *Abca12*^{-/-} mice (Figure 1B) were typically born with a smaller body size than that of wild-type mice (Figure 1A). Erythematous, rigid skin covered the entire body surface of *Abca12*^{-/-} neonates.

Light microscopy showed a thick, compact cornified layers without the normal basket-weave appearance in the *Abca12*^{-/-} neonatal skin (Figure 1D), compared with normal neonatal skin (Figure 1C). Electron microscopy of *Abca12*^{-/-} neonatal skin showed numerous lipid droplets in the granular layer cell cytoplasm (Figure 1F). In wild-type neonatal skin, no lipid droplets were seen although normal keratohyalin granules were observed (Figure 1E). Immunofluorescence staining (Figure 1, G and H)



K Total ceramide in *Abca12*^{-/-} and control neonates



showed *Abca12* in wild-type but not *abca12*^{-/-} mice, with the glucosylceramide/ceramide distribution remarkably sparse at the *Abca12*^{-/-} neonatal mice granular/cornified layer interface (Figure 1J), compared with the intense labeling in the wild-type neonatal epidermis (Figure 1I). To verify these results in the neonatal *Abca12*^{-/-} and wild-type skin, we performed lipid analysis using skin samples from both the *Abca12*^{-/-} and wild-type neonates. Total amounts of epidermal ceramides were significantly reduced in *Abca12*^{-/-} neonatal mice (Figure 1K). Particularly, amounts/compositions of the CER[EOS], ceramide classes consisting of ester-linked non-hydroxy fatty acids, ω -hydroxy fatty acids and 4-sphingenines, in *Abca12*^{-/-} neonatal epidermis were extremely small compared with control mice (see Supplemental Figure S1, A and B at <http://ajp.amjpathol.org>).

Immunofluorescence staining revealed that the keratinocyte differentiation (keratinization)-specific molecules, kallikrein 5 (KLK5), transglutaminase 1 (TGase1), and loricrin, were sparsely distributed in the upper epidermis of neonatal *Abca12*^{-/-} mice (Figure 2A–J). Immunofluorescence staining for KLK5, a lamellar granule component, was weak in *Abca12*^{-/-} neonatal mice granular layer (Figure 2B), in contrast to intense labeling in granular and lower cornified layers of wild-type neonatal skin (Figure 2A). *In situ* TGase1 activity assays with dansylcadaverine as a substrate showed neonatal *Abca12*^{-/-} granular layer keratinocytes exhibited weak TGase1 activity restricted to the cytoplasm (Figure 2D), compared with distinct TGase1 activity with a more peripheral pattern throughout neonatal wild-type granular layer keratinocytes (Figure 2C). Immunofluorescence staining showed loricrin expressed sparsely within neonatal *Abca12*^{-/-} granular layer cells (Figure 2F), compared with more intense expression in neonatal wild-type granular layer keratinocytes (Figure 2E).

KLK5, involucrin, TGase1, loricrin, and filaggrin mRNA expression was up-regulated in neonatal *Abca12*^{-/-} epidermal keratinocytes (Figure 2K). In contrast, protein expression using epidermal extract, Western blotting demonstrated that loricrin and KLK5 protein expression was reduced in neonatal *Abca12*^{-/-} epidermal keratinocytes compared with that in neonatal wild-type epidermis (Figure 2L). There were no significant differences in the pro-

Figure 1. *Abca12*^{-/-} neonatal phenotype and lipid trafficking defects. **A** and **B:** Gross phenotypes of wild-type and *Abca12*^{-/-} neonates. **C** and **D:** Light microscopy showed a thick compact cornified layer (bracket) without the normal basket-weave appearance in the *Abca12*^{-/-} mouse skin (**D**), compared with normal neonatal skin (**C**) (H&E stain; original magnification, $\times 40$) (Scale bars = 20 μ m). **E** and **F:** An electron micrograph of the *Abca12*^{-/-} neonatal skin showed numerous lipid droplets in the cytoplasm of the granular layer cells (**F**, red arrows). In the wild-type neonatal skin, no lipid droplets were seen and normal keratohyalin granules were observed (**E**, red arrows) (original magnification, $\times 3000$) (Scale bars = 2 μ m). **G** and **H:** By immunofluorescence staining, *Abca12* expression (Alexa488, green) was detected in the wild-type neonatal mouse skin (**G**), but not in the *Abca12*^{-/-} skin (**H**). **I** and **J:** Immunofluorescence staining showed the glucosylceramide/ceramide (GlcCer/Cer) (Alexa 488, green), a major lipid component of lamellar granules and an essential component of the epidermal permeability barrier, to be distributed remarkably sparse in the *Abca12*^{-/-} neonatal mouse granular/cornified layer interface (**J**), compared with the intense labeling in the wild-type neonatal epidermis (**I**). **K:** In neonatal mice, total ceramides levels were significantly reduced in the epidermis of *Abca12*^{-/-} mice. (*Abca12*^{-/-} neonates, $n = 3$; control neonates, $n = 2$) ($*P < 0.01$). GlcCer, glucosylceramide; Cer, ceramide.

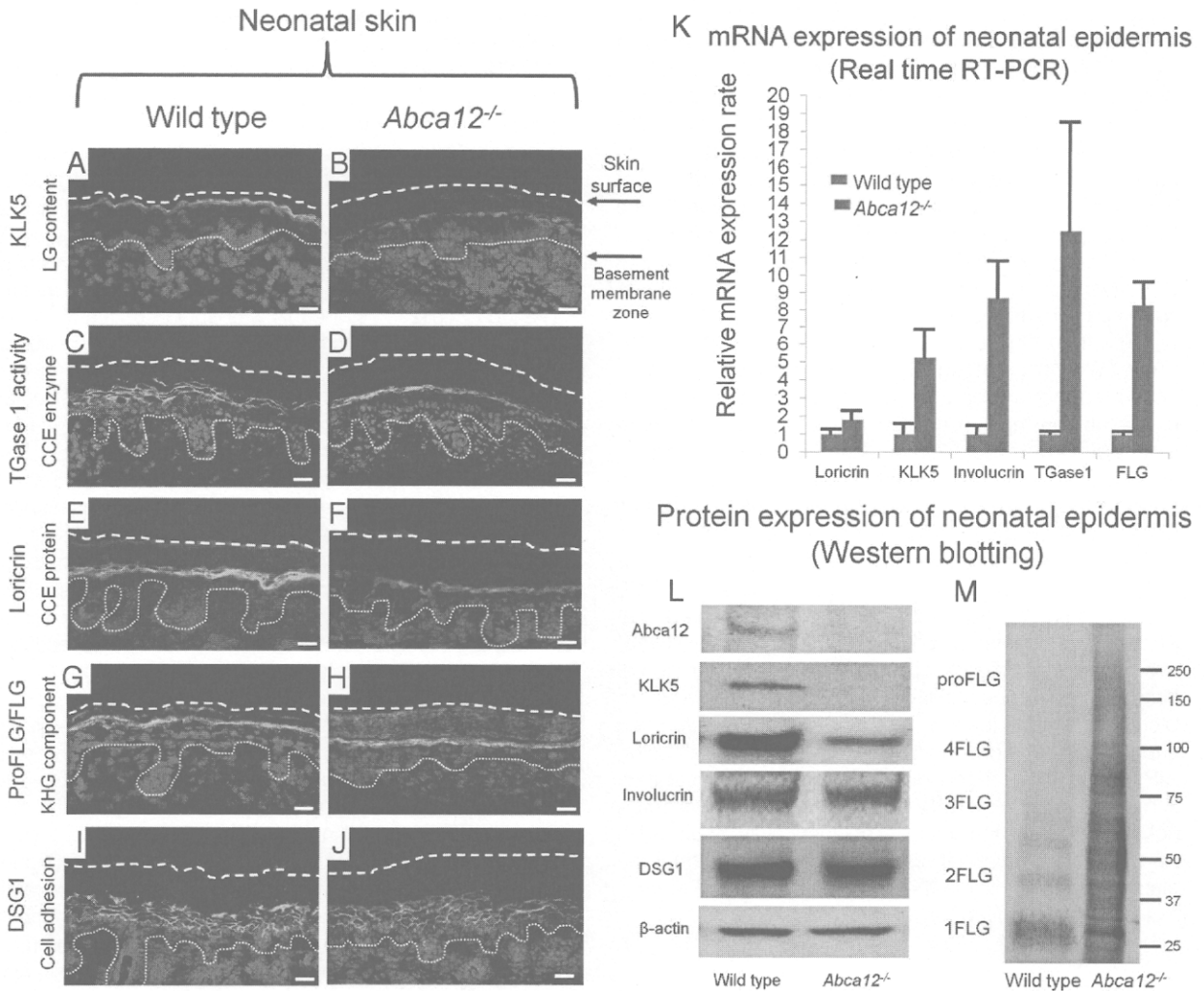


Figure 2. Reduced epidermal differentiation-associated molecules and defective conversion of profilaggrin to filaggrin in *Abca12*^{-/-} neonates. **A and B:** Immunofluorescence staining for kallikrein 5 (KLK5) (Alexa488, green), one of the lamellar granule (LG) contents, was weak in the *Abca12*^{-/-} neonatal mice granular keratinocyte layers (**B**), in contrast to its intense labeling in the granular layers and lower cornified layers of wild-type neonatal skin (**A**). **C and D:** *In situ* transglutaminase 1 (TGase1) activity assay (fluorescein isothiocyanate, green) with dansyl-cadaverine showed the granular layer keratinocytes in the *Abca12*^{-/-} neonates had weak transglutaminase 1 activity only in the cytoplasm (**D**), compared with distinct transglutaminase 1 activity with the peripheral pattern throughout granular layer keratinocytes in the wild-type neonates (**C**). Cytoplasmic localization of transglutaminase 1 in *Abca12*^{-/-} neonates indicated its inability to bind to the cell membrane and to therefore function at its proper place despite the significantly enhanced mRNA expression of transglutaminase 1 (see Figure 2K). **E and F:** Immunofluorescence staining showed loricrin (Alexa 488, green) expressed sparsely in the *Abca12*^{-/-} neonatal mice granular layer (**F**), compared with its intense expression in the granular layer of the wild-type neonatal skin (**E**). **G and H:** Both *Abca12*^{-/-} and wild-type neonatal skin showed intense profilaggrin/filaggrin (proFLG/FLG) (Alexa488, green) expression in the granular layer keratinocytes. However, in *Abca12*^{-/-} neonatal skin, profilaggrin/filaggrin distribution was also observed throughout the cornified layers. **I and J:** Desmoglein 1 (DSG1) (Alexa 488, green), a cell adhesion molecule unassociated with keratinization, was expressed at the cell periphery in the lower granular and spinous layers of the both *Abca12*^{-/-} neonatal skin and wild-type mouse skin. (nuclear stain; propidium iodide, red, **dotted lines**, the skin surface). Original magnification $\times 40$; Scale bars, 20 μ m. **K:** mRNA expression of loricrin, kallikrein 5 (KLK5), involucrin, transglutaminase 1 (TGase1) and filaggrin (FLG) was up-regulated in the *Abca12*^{-/-} neonatal epidermis. (*Abca12*^{-/-} neonates, *n* = 5; wild-type neonates, *n* = 5, mRNA expression levels of wild-type neonatal epidermis = 1). **L:** Western blotting of epidermal extracts showed that protein expression of kallikrein 5 (KLK5) and loricrin was lower in the *Abca12*^{-/-} neonatal epidermis (right) than in the wild-type neonatal epidermis (left). There were no significant differences of desmoglein 1 (DSG1), involucrin, β -actin expressions between the *Abca12*^{-/-} and wild-type epidermis. **M:** Western blotting with anti-profilaggrin/filaggrin antibody revealed the *Abca12*^{-/-} neonatal epidermis (right) expressed more profilaggrin/filaggrin protein than wild-type neonatal epidermis (left). High molecular weight smear band corresponding to non-converted profilaggrin peptides were characteristic to the *Abca12*^{-/-} neonatal epidermis. Western blotting using serial protein dilutions is shown in the supplemental Figure 2 (see Supplemental Figure S2 at <http://ajp.amjpatol.org>). KLK5, kallikrein 5; LG, lamellar granule; TGase1, transglutaminase 1; CCE, cornified cell envelope; FLG, filaggrin; KHG, keratohyalin granule; DSG1, desmoglein 1; proFLG, profilaggrin; 4FLG, filaggrin tetramer; 3FLG, filaggrin trimer; 2FLG, filaggrin dimer; 1FLG, filaggrin monomer.

tein expression of involucrin or control molecules unconnected with the keratinization process, β -actin, and desmoglein1 (DSG1), between *Abca12*^{-/-} and wild-type neonatal epidermis.

Both *Abca12*^{-/-} and wild-type neonatal skin demonstrated intense profilaggrin/filaggrin expression within granular layer keratinocytes (Figure 2, G and H). However, in

Abca12^{-/-} neonatal skin, profilaggrin/filaggrin distribution was also observed throughout all of the cornified layers (Figure 2H). Western blotting with anti-profilaggrin/filaggrin antibody revealed that neonatal *Abca12*^{-/-} epidermis exhibited a greater amount of profilaggrin/filaggrin protein than that in the neonatal wild-type epidermis (Figure 2M). In particular, high molecular weight smear bands correspond-

ing to unconverted profilaggrin peptides were characteristic of neonatal *Abca12*^{-/-} epidermis. Western blotting using the serial dilutions of protein showed that neonatal *Abca12*^{-/-} epidermis exhibited a filaggrin monomer band, although the ratio of high molecular weight profilaggrin and its derivatives to filaggrin monomer in the *Abca12*^{-/-} neonatal epidermis was extremely high compared with that of the wild-type neonatal epidermis (see Supplemental Figure S2A at <http://ajp.amjpathol.org>). The remaining high molecular bands in the neonatal *Abca12*^{-/-} epidermis indicated defective profilaggrin conversion to filaggrin. Furthermore, we prepared 8 mol/L urea supernatants from precipitated proteins from the *Abca12*^{-/-} neonatal epidermis in RIPA buffer. Western blotting with 8 mol/L urea supernatants confirmed that a proportion of filaggrin monomer, which is insoluble in the RIPA buffer exists in *Abca12*^{-/-} neonatal epidermis (see Supplemental Figure S2B at <http://ajp.amjpathol.org>). In contrast, urea supernatants from precipitated proteins in RIPA buffer of wild-type neonatal epidermis showed only a faint band of filaggrin monomer. This finding indicated that majority of filaggrin monomer in the wild-type neonatal epidermis is soluble in RIPA buffer. These Western blotting results suggested that *Abca12*^{-/-} neonatal epidermis exhibited not only defective profilaggrin/filaggrin conversion but also alteration of filaggrin monomer solubility. We also performed Western blotting with anti-loricrin antibody using 8 mol/L urea supernatant. Using 8 mol/L urea buffer as well as using RIPA buffer the loricrin band was faint in supernatant samples from the *Abca12*^{-/-} neonatal epidermis (data not shown). Thus, the solubility of loricrin was unaltered in the *Abca12*^{-/-} neonatal epidermis and we think that the alteration of solubility in the *Abca12*^{-/-} neonatal epidermis is specific to filaggrin.

Improved Morphological Abnormalities, Corrected Lipid Distribution, and Restored Expression of Differentiation-Specific Molecules in Abca12^{-/-} Skin Grafts Maintained in Dry Environment

Since *Abca12*^{-/-} neonates die soon after birth, it was impossible to follow the phenotypic changes in the skin of *Abca12*^{-/-} mice after birth. Therefore, we grafted their skin onto severe combined immunodeficient (SCID) mice and analyzed its morphological and biochemical alterations in the skin after birth/grafting.

Mature grafted *Abca12*^{-/-} skin showed hairless keratotic plates at 3 weeks after transplantation onto the backs of SCID mice (Figure 3, A and B). Light microscopic observations revealed that hair follicles and shafts were buried in keratotic plugs in mature *Abca12*^{-/-} skin (Figure 3, C and D). High power microscopy demonstrated that mature *Abca12*^{-/-} skin showed discernible keratohyalin granules in the granular layers (Figure 3F) that were completely absent in *Abca12*^{-/-} neonatal skin (Figure 1, E and F).

Immunofluorescence staining showed *abca12* staining in wild-type but not *abca12*^{-/-} mice and intense labeling of glucosylceramides/ceramides at the granular/cornified

layer interface in mature grafted *Abca12*^{-/-} skin (Figure 3, I and J), compared with a sparse distribution in the neonatal *Abca12*^{-/-} mouse upper epidermis (Figure 1L). Electron microscopy of mature *Abca12*^{-/-} skin showed many lipid droplets in the granular layer (Figure 3K), although the number of lipid droplets in the cornified layer was reduced when compared with that of neonatal skin (Figure 3L). Using lipid analysis, the amounts of both total ceramides and CER[EOS] were restored in mature *Abca12*^{-/-} epidermis (Figure 3M, and see Supplemental Figure S1, C and D at <http://ajp.amjpathol.org>). These results indicate that mature grafted *Abca12*^{-/-} epidermis was able to obtain a normal ceramide distribution together with a normal composition of ceramides.

Immunolabeling for differentiation-specific molecules confirmed improved keratinization during maturation of the grafted *Abca12*^{-/-} skin (Figure 4, A–J). Intense KLK5 immunolabeling (Figure 4, A and B), *in situ* transglutaminase 1 (TGase1) activity (Figure 4, C and D), and loricrin immunostaining (Figure 4, E and F) were distributed throughout the granular layers in mature grafted *Abca12*^{-/-} skin, compared with a sparse distribution in *Abca12*^{-/-} neonatal skin (Figure 2, B, D, and F). Increased loricrin and KLK5 immunolabeling intensity was confirmed by Western blot analysis using epidermal extracts from mature grafted *Abca12*^{-/-} epidermis (Figure 4K).

Mature grafted *Abca12*^{-/-} skin showed intense profilaggrin/filaggrin labeling in the granular layer (Figure 4H), similar to the mature grafted wild-type skin (Figure 4G). The diffuse profilaggrin/filaggrin distribution throughout the cornified layers observed in *Abca12*^{-/-} neonatal skin (Figure 2H) was not seen in mature grafted *Abca12*^{-/-} skin (Figure 4H). Western blotting with anti-profilaggrin/filaggrin antibody revealed that the normal conversion of profilaggrin to filaggrin was restored in mature *Abca12*^{-/-} epidermis (Figure 4K). Epidermal extracts of mature *Abca12*^{-/-} skin at 3 weeks after transplantation showed low expression of high molecular weight smeared bands and, instead of those, exhibited intense filaggrin monomer bands, compared those with epidermal extracts of *Abca12*^{-/-} neonatal skin.

Analysis of TEWL as a parameter of skin barrier defects, demonstrated *Abca12*^{-/-} that neonatal back skin showed significantly greater TEWL than the wild-type neonatal skin ($n = 3$, $P < 0.001$) (Figure 4L). However, TEWL levels of mature *Abca12*^{-/-} skin 3 weeks after the skin graft were significantly decreased as compared with levels of *Abca12*^{-/-} neonatal skin ($n = 3$, $P < 0.001$).

Subcultured Abca12^{-/-} Mouse Keratinocytes Attained Normal Lipid Trafficking in the Cytoplasm, with Restoration of Differentiation-Specific Protein Expression and Intact Profilaggrin/Filaggrin Conversion that Was Defective in Primary-Cultured *Abca12*^{-/-} Mouse Keratinocytes

To verify the results from grafted skin analysis, we performed a similar analysis using primary versus subcultured *Abca12*^{-/-} keratinocytes. Immunolabeling with an-

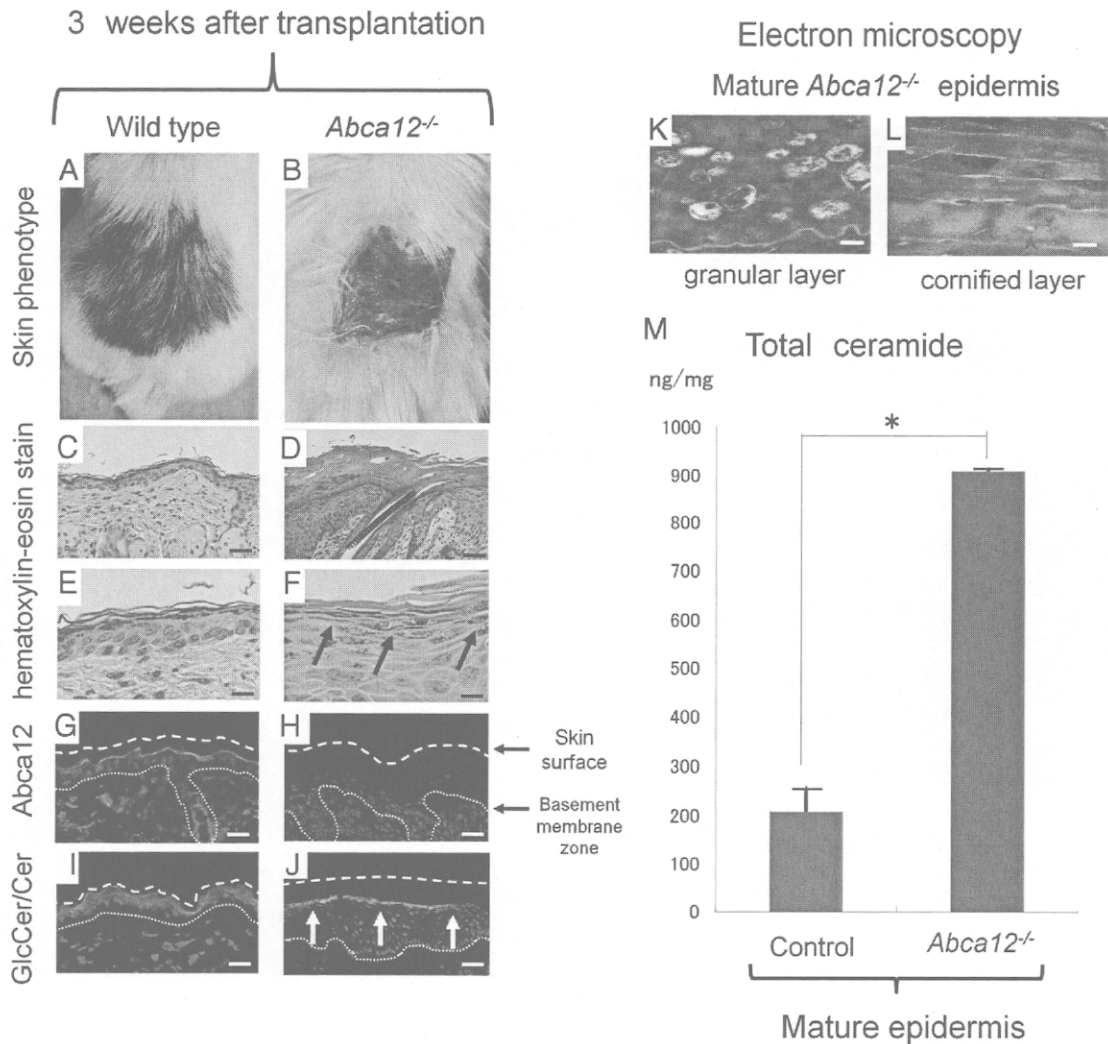


Figure 3. Altered morphology and improvement of ceramide deficiency during maturation of *Abca12*^{-/-} skin. Gross (A and B) and microscopic (C-L) appearances of wild-type and *Abca12*^{-/-} skin three weeks after transplantation onto SCID mice. **A:** Grafted skin of wild-type mice three weeks after transplantation. **B:** Grafted *Abca12*^{-/-} skin three weeks after transplantation showed hairless keratotic plates. **C and D:** Light microscopic observation histology (H&E stain; original magnification $\times 40$; Scale bars = 20 μm). Hair follicles and shafts were buried in keratotic plugs in the mature *Abca12*^{-/-} skin three weeks after the skin graft (**D**). **E and F:** High power views (H&E stain; original magnification $\times 60$; Scale bars = 10 μm). Mature *Abca12*^{-/-} skin three weeks after transplantation showed discernible keratohyalin granule in the granular layers (**F**, arrows) that were lacked in *Abca12*^{-/-} neonatal skin (see Figure 1, D and F). **G and H:** By immunofluorescence staining, *Abca12* expression (Alexa488, green) was detected in the mature wild-type mouse skin (**G**), but not in the mature *Abca12*^{-/-} skin (**H**). **I and J:** Immunofluorescence staining showed an intense distribution of glucosylceramide/ceramide (GlcCer/Cer) (Alexa 488, green) at the granular/cornified layer interface in mature *Abca12*^{-/-} epidermis (**J**, arrows), compared with a sparse distribution in the neonatal *Abca12*^{-/-} mouse upper epidermis (see Figure 1J). **K and L:** Ultrastructural observation of the grafted *Abca12*^{-/-} skins three weeks after transplantation. There were many lipid droplets in the granular layer (**K**, red arrowheads), however the number of lipid droplets in the cornified layer (**L**, red arrowheads) was fewer than that of the neonatal *Abca12*^{-/-} skin (see Figure 1F). Original magnification: $\times 10000$ (**K**), $\times 5000$ (**L**); Scale bars: 100 nm (**K**), 200 nm (**L**). **M:** From the lipid analysis of grafted skins, total ceramides levels of mature *Abca12*^{-/-} epidermis were restored. (*Abca12*^{-/-} grafted skins, $n = 2$; control grafted skins, $n = 2$) ($*P < 0.01$). GlcCer, glucosylceramide; Cer, ceramide

ti-glucosylceramide/ceramide antibody demonstrated a congested glucosylceramide/ceramide pattern in differentiated primary-cultured *Abca12*^{-/-} mouse keratinocytes after first passage (Figure 5, B and E), compared with an uncongested, diffuse peripheral glucosylceramide/ceramide pattern in differentiated primary-cultured wild-type mouse keratinocytes (Figure 5, A and D). After 10 passages, subcultured *Abca12*^{-/-} keratinocytes showed a widely distributed, diffuse glucosylceramide/ceramide staining pattern, similar to those of primary-cultured wild-type keratinocytes (Figure 5, C and F). Subcultured wild-type keratinocytes after 10 passages failed

to show any alterations in lipid distribution (data not shown). These results indicate that lipid trafficking recovered during 10 passages of subculture in our *Abca12*^{-/-} keratinocytes.

To investigate this altered differentiation state of primary/subcultured *Abca12*^{-/-} keratinocytes, we performed real-time RT-PCR and immunoblot analysis (Figure 5, G and H). No significant differences were obtained in loricrin, KLK5, involucrin, TGase1 and filaggrin mRNA expression between primary-cultured *Abca12*^{-/-} and wild-type keratinocytes (Figure 5G). Subcultured *Abca12*^{-/-} keratinocytes showed higher loricrin, KLK5 and TGase1 mRNA

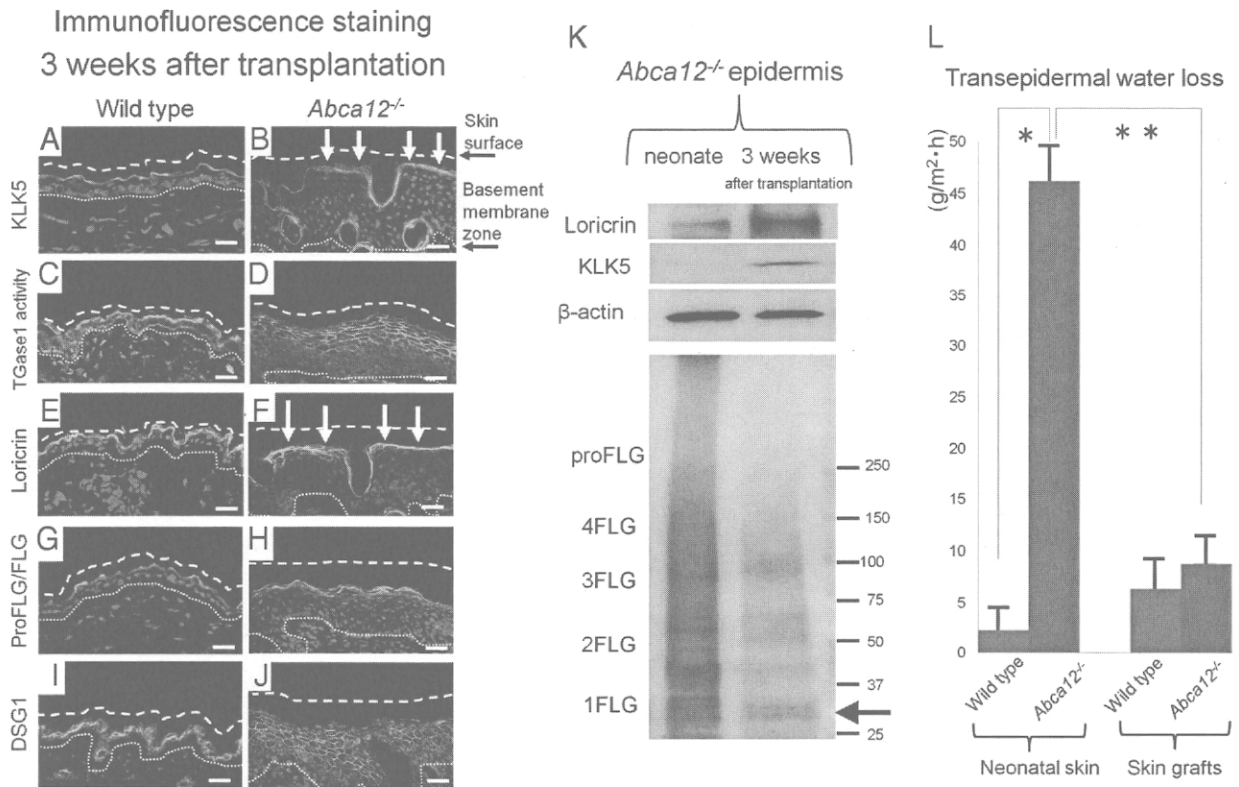


Figure 4. Improvement of previously disrupted differentiation-specific protein expression and defective skin barrier function in postnatal *Abca12*^{-/-} skin. **A–J:** Immunolabeling for differentiation-specific molecules confirmed improved keratinization during maturation of the grafted *Abca12*^{-/-} skin. Intense kallikrein 5 (KLK5) immunostaining (**A** and **B**, white arrows), *in situ* transglutaminase 1 (TGase1) activity labeling (**C** and **D**) and loricrin immunolabeling (**E** and **F**, white arrows) were seen throughout the granular layers in mature grafted *Abca12*^{-/-} skin, compared with their sparse distribution in the *Abca12*^{-/-} neonatal skin (see Figure 2, B, D and F). Increased loricrin and KLK5 immunolabeling intensity was confirmed by Western blot analysis using epidermal extracts from mature grafted *Abca12*^{-/-} skin (**K**). Mature grafted *Abca12*^{-/-} skin showed intense profilaggrin/filaggrin labeling in the granular layer (**H**), similar to the mature grafted wild-type skin (**G**). Diffuse profilaggrin/filaggrin staining in the entire cornified layers observed in *Abca12*^{-/-} neonatal skin (see Figure 2H) disappeared in mature grafted *Abca12*^{-/-} skin. Expression of desmoglein 1 (DSG1), unassociated with keratinization, was not altered in the grafted skin (**I** and **J**). Western blotting with anti-profilaggrin/filaggrin antibody revealed that normal conversion of profilaggrin to filaggrin was restored in mature *Abca12*^{-/-} epidermis (**K**). Nuclear stain: propidium iodide, red; original magnification ×40; Scale bars = 20 μm. **L:** The barrier function in the transplanted skin was assessed by measuring transepidermal water loss (TEWL). The *Abca12*^{-/-} neonates (red bar, left) showed significantly greater TEWL than the wild-type neonates (blue bar, left) showed (**P* < 0.001). TEWL levels of mature *Abca12*^{-/-} epidermis three weeks after the skin graft (red bar, right) were significantly decreased as compared with levels of *Abca12*^{-/-} neonatal skin (red bar, left) (***P* < 0.001), and was similar to levels of mature wild-type skin three weeks after the skin graft (blue bar, right). (*Abca12*^{-/-} neonates, *n* = 3; wild-type neonates, *n* = 3; mature *Abca12*^{-/-} skin, *n* = 3; mature wild-type skin, *n* = 3). KLK5, kallikrein 5; proFLG, profilaggrin; FLG, filaggrin; 4FLG, filaggrin tetramer; 3FLG, filaggrin trimer; 2FLG, filaggrin dimer; 1FLG, filaggrin monomer.

levels compared with primary-cultured *Abca12*^{-/-} keratinocytes (Figure 5G). Blot extracts from differentiated primary-cultured *Abca12*^{-/-} keratinocytes showed low expression of loricrin and KLK5 (Figure 5H), as observed in neonatal *Abca12*^{-/-} mice epidermis (Figure 2L). However, extracts from subcultured *Abca12*^{-/-} keratinocytes showed restoration of loricrin and KLK5 expression (Figure 5H), as observed in grafted mice epidermis (Figure 4K).

Western blotting with anti-profilaggrin/filaggrin antibody revealed that the filaggrin expression pattern had become normalized in subcultured *Abca12*^{-/-} keratinocytes (Figure 5H). Cell lysates from 10 passage-subcultured *Abca12*^{-/-} keratinocytes showed an intense filaggrin monomer band that was faint in lysates from *Abca12*^{-/-} primary first-passage keratinocytes.

Studies of subcultured *Abca12*^{-/-} keratinocytes demonstrated restored differentiation, at least in part, similar to that observed in mature *Abca12*^{-/-} skin grafts.

cDNA Microarray Analysis Revealed Up-Regulation of 22 Lipid Metabolic and/or Transport-Related Genes

To investigate the mechanism of restoration of intact keratinocytes differentiation in subcultured *Abca12*^{-/-} keratinocytes, we analyzed whole gene expression profile of primary/subcultured *Abca12*^{-/-} keratinocytes maintained under high Ca²⁺ condition using cDNA microarray methods. We obtained the 35,582 gene expression profile and observed 566 transcripts that were up-regulated more than three-fold in subcultured *Abca12*^{-/-} keratinocytes compared with primary-cultured *Abca12*^{-/-} keratinocytes. Among them, we searched for genes related to “lipid metabolism and/or lipid transporter function,” and identified 22 specific transcripts including solute carrier family 22 member 7 (*Slc22a7*), prostaglandin D2 syn-

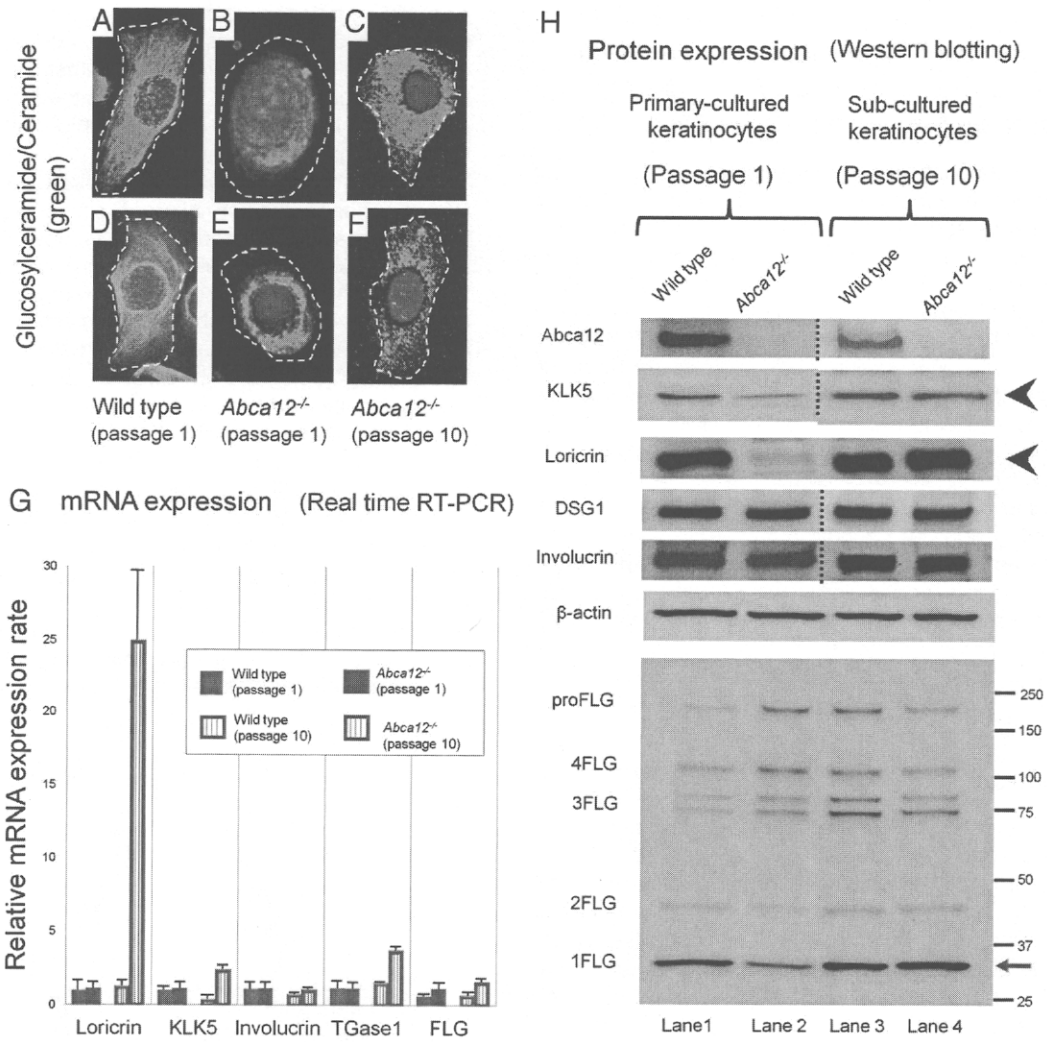


Figure 5. Subcultured *Abca12*^{-/-} mouse keratinocytes exhibited restored intracytoplasmic localization of glucosylceramide/ceramide, protein expression of differentiation-specific molecules and profilaggrin conversion. **A–F:** Intracytoplasmic localization of glucosylceramide/ceramide in cultured keratinocytes. Immunolabeling demonstrated a congested pattern of glucosylceramide/ceramide (Alexa 488, green) in differentiated primary-cultured *Abca12*^{-/-} mouse keratinocytes after first passage (**B** and **E**), in contrast with the uncongested, diffuse, peripheral pattern in the differentiated keratinocytes of a wild-type mouse (**A** and **D**). After 10 passages, subcultured *Abca12*^{-/-} keratinocytes showed a widely distributed, diffuse glucosylceramide staining pattern (**C** and **F**), similar to those of wild-type keratinocytes. Subcultured wild-type keratinocytes after ten passages did not show any alterations in lipid distribution (data not shown). Nuclear stain: propidium iodide, red; original magnification ×60. **Dotted lines** are the cell surface. **G:** There were no significant differences in loricrin, kallikrein 5 (KLK5), involucrin, transglutaminase 1 (TGase1), and filaggrin (FLG) mRNA expression between primary-cultured *Abca12*^{-/-} keratinocytes (red bars, left) and primary-cultured wild-type keratinocytes (blue bars, left). Subcultured *Abca12*^{-/-} keratinocytes (red bars, right) and subcultured wild-type keratinocytes (blue bars, right) showed higher mRNA levels of loricrin, kallikrein 5, and transglutaminase 1 compared with primary-cultured *Abca12*^{-/-} keratinocytes (red bars, left) and subcultured wild-type keratinocytes (blue bars, right). No significant difference was observed in involucrin and filaggrin mRNA expression. (primary-cultured *Abca12*^{-/-}, *n* = 5; primary-cultured wild-type, *n* = 5; subcultured *Abca12*^{-/-}, *n* = 5; subcultured wild-type, *n* = 5; mRNA expression levels of *Abca12*^{-/-} primary cultured keratinocytes = 1). **H:** Western blotting of differentiated cultured keratinocytes lysates under high Ca²⁺ condition showed that loricrin and KLK5 expression was lower in *Abca12*^{-/-} primary-cultured keratinocytes (**lane 2**) than that of the wild-type primary-cultured keratinocytes (**lane 1**). Extracts from subcultured *Abca12*^{-/-} keratinocytes showed restoration of loricrin and KLK5 expression (**lane 4**, **black arrowheads**). Western blotting with anti-profilaggrin/filaggrin antibody revealed that the *Abca12*^{-/-} primary-cultured keratinocytes (**lane 2**) had reduced expression of mature filaggrin monomer than the wild-type primary-cultured keratinocytes (**lane 1**). In addition, the lysate from *Abca12*^{-/-} primary-cultured keratinocytes exhibited plenty of high molecular weight bands, which indicated profilaggrin expression (**lane 2**). The filaggrin expression pattern was normalized in subcultured *Abca12*^{-/-} keratinocytes (**lane 4**). Cell lysates from subcultured *Abca12*^{-/-} keratinocytes showed an intense filaggrin monomer band that was faint in lysates from *Abca12*^{-/-} primary first-passage keratinocytes (**lane 2** and **4**, **red arrow**). KLK5, kallikrein 5; TGase, transglutaminase; DSG1, desmoglein 1; proFLG, profilaggrin; 4FLG, filaggrin tetramer; 3FLG, filaggrin trimer; 2FLG, filaggrin dimer; 1FLG, filaggrin monomer.

thetase (*Ptgds*), annexin A9 (*Anxa9*), bactericidal/permeability-increasing protein-like 2 (*Bpil2*), phosphatidylethanolamine binding protein-2 variant 1 homolog (*Pbp2*), lipocalin 7 (*Tinagl*), *Gpr119*, solute carrier family 5 member 1 (*Slc5a1*), prostaglandin-endoperoxide synthase 2

(*Ptg2*), and solute carrier family 30 member 1 (*Slc30a1*) (see Supplemental Table S1 at <http://ajp.amjpathol.org>). Notably, these genes included four ATP-binding transporter family members: *Abca17*, *Abca1a*, *Abcc5*, and *Abcb11* that were up-regulated at least three-fold.

Keratinocytes Treated with Retinoids Failed to Exhibit Normal Differentiation and Therapeutic Trials onto Grafted HI Model Mice Failed to Demonstrate Skin Phenotype Recovery

As treatment trials for primary keratinocytes, Western blotting revealed that primary-cultured wild-type keratinocytes expressed a large amount of loricrin peptide and had a decent amount of filaggrin monomer converted from profilaggrin (see Supplemental Figure S3 at <http://ajp.amjpathol.org>). Both isotretinoin (10^{-6} mol/L) and etretinate (10^{-6} mol/L) in the cultured medium for 48 hours lead to remarkable reduction of loricrin protein expression in primary-cultured wild-type keratinocytes, although filaggrin expression patterns were not altered. Neither isotretinoin (10^{-6} mol/L) nor etretinate (10^{-6} mol/L) improved the deficient loricrin protein expression or defective profilaggrin conversion in the primary-cultured *Abca12*^{-/-} keratinocytes under high Ca²⁺ condition.

As a treatment trial for HI grafted skin, oral administration of various doses of isotretinoin (1 or 10 mg/kg daily for 10 consecutive days) to HI skin graft-recipient SCID mice demonstrated no change in the skin phenotype of grafted HI model mice skin at all (data not shown).

Discussion

Keratinocyte terminal differentiation (keratinization) is remarkably important to skin physiology and essential for epidermal function including barrier formation. Keratinization is a highly regulated process, involving a number of genes and pathways. Until now, abnormalities in keratinocyte differentiation have been reported in HI patients. Morphologically, Buxman et al¹⁰ have reported that granular layers were absent or poorly formed in HI patient epidermis. Dale et al reported abnormal lamellar granules and defective profilaggrin conversion both in HI patients skin and their cultured keratinocytes.¹¹ Profilaggrin conversion to filaggrin is a key step during epidermal keratinization. Fleckman et al¹² reported that HI keratinocytes in 3 dimensional culture were unable to show the adequate differentiated epithelium and profilaggrin/filaggrin conversion. Recently, Thomas et al reported that the desquamation specific enzyme, kallikrein 5, and cathepsin D, were remarkably reduced in HI model skin using ABCA12 small interfering RNA knockdown keratinocytes.¹³

In the present study, we have demonstrated that keratinocyte differentiation was severely disrupted in both *Abca12*^{-/-} HI neonatal model mouse skin and primary-cultured *Abca12*^{-/-} keratinocytes. The present findings were consistent with previous reports of findings in HI patient's skin. Our neonatal HI model mice skin showed no apparent keratohyalin granules within any of their granular layer cells, which was consistent with Buxman's study.¹⁰ Furthermore, our immunoblotting results confirmed defective profilaggrin/filaggrin conversion, which was consistent with the studies by Dale et al¹¹ and Fleckman et al.¹² Our immunostaining and immunoblotting results showed reduced expression of KLK5 in neonatal

Abca12^{-/-} epidermis and primary-cultured *Abca12*^{-/-} keratinocytes, which was consistent with the study by Thomas et al.¹³ We therefore believe that our *Abca12*^{-/-} HI model mouse faithfully reproduces the molecular condition thus far identified in human HI epidermis in addition to mimicking clinical phenotype.⁵

Zuo et al⁶ suggested that loss of ABCA12 did not induce a block in the normal processing of profilaggrin to filaggrin in another reported ABCA12 deficient mouse strain, although the solubility of filaggrin was altered. We believe that our data are consistent with Zuo's study. In the present study, we showed high molecular weight bands in RIPA buffer extracted supernatant from neonatal *Abca12*^{-/-} epidermis. In study by Zuo et al,⁶ similar high molecular weight bands were also seen by the Western blotting after detergent buffer supernatant extraction. We also showed an alteration in filaggrin monomer solubility using 8 mol/L urea supernatant, reproducing the findings of Zuo et al.⁶ The major difference between these two studies is that Zuo et al⁶ showed no filaggrin monomer band after detergent buffer supernatant extraction in their ABCA12 deficient mouse skin. In contrast, we detected filaggrin monomer band in RIPA supernatant of our *Abca12*^{-/-} neonatal epidermis. This finding might result from differences in lysis buffer, tissue sample

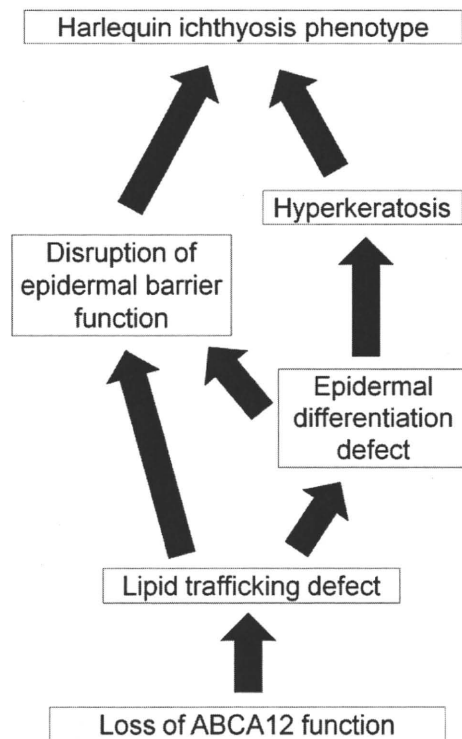


Figure 6. Putative pathomechanism of harlequin ichthyosis. Based on our results, we propose a novel pathogenetic mechanism underlying harlequin ichthyosis (HI). Our results suggested that a lipid trafficking defect due to loss of ABCA12 function leads to not only malformation of the epidermal lipid barrier but also "an epidermal differentiation defect." In our hypothesis, the severe hyperkeratosis, a characteristic phenotype of HI skin, is not a hyperkeratosis compensating for any barrier insufficiency, but a hyperkeratosis due to both defective differentiation and an abnormal desquamation process. The present scenario explains both the HI skin phenotype at/after birth and even *in utero*.

(whole skin or only epidermis), or harvest time (E18.5 or neonate). We conclude that neonatal *Abca12*^{-/-} epidermis exhibits not only defective profilaggrin/filaggrin conversion but also alterations in filaggrin monomer solubility, as previously suggested by Dale et al,¹¹ Fleckman et al,¹² and Zuo et al.⁶

Based on our results, we propose several new pathogenic mechanisms for HI (Figure 6). Our results suggest that "an epidermal differentiation defect" is the major pathomechanism in HI. This new pathogenesis model is furthermore able to resolve the conflicting "the barrier insufficiency" theory with the (human) HI clinical phenotype. Our novel "epidermal differentiation" theory can explain HI skin phenotype at birth and even *in utero*. In our theory, severe hyperkeratosis, characteristic of the HI skin phenotype, was not a compensative hyperkeratosis for barrier insufficiency, but a hyperkeratosis due to defective differentiation and desquamation processes.

Epidermal differentiation defects in our HI model mice suggest that ABCA12 lipid trafficking, which occurs during the early stages of keratinization, is a crucial step for correct keratinocyte terminal differentiation. In normal granular layer keratinocytes, ABCA12 transports lipids and forms lamellar granules.³ Just after the extrusion of lipids from lamellar granules at the granular/cornified layer interface, loricrin accumulates at the cell periphery and is integrated into the insoluble cornified cell envelope by transglutaminases.¹⁴ At the final phase of terminal differentiation, profilaggrin undergoes many post-translational modifications, including conversion to functional filaggrin monomers, which aid in the bundling of keratin intermediate filaments and formation of the cornified cell envelope.¹⁴⁻¹⁶ Serine proteases including KLK5 are involved in the desquamation process after keratinization.¹⁷ Our present results suggest that defective lipid trafficking and lamellar granule formation fail to initiate the normal sequence of events of the keratinization process. These facts indicate that ABCA12 lipid trafficking is essential to precisely regulate keratinocyte differentiation.

Interestingly, mature grafted HI model mouse skin and subcultured *Abca12*^{-/-} keratinocytes showed improvement in the *Abca12*^{-/-}-related abnormalities observed in neonatal skin and primary-cultured keratinocytes, such as the aberrant ceramide distribution, reduced differentiation-specific protein expression and profilaggrin/filaggrin conversion defects. Similar to our *Abca12*^{-/-} model mouse skin, improvement in skin manifestations during maturation was observed in several other ichthyotic model mice. Loricrin knockout mice exhibit shiny translucent skin at birth although these mice showed a normal skin phenotype at 4 to 5 days after birth.¹⁸ Biochemically, the mice showed increased protein expression of small proline rich proteins, which are also cornified cell envelope components during skin maturation.¹⁸ Mature 12R-lipoxygenase knockout mouse skin showed recovery of skin barrier function and restoration of profilaggrin conversion after maturation, which had been lacking in the neonatal mice.^{19,20} In addition, mature transglutaminase 1 knockout mouse skin also showed skin barrier functional recovery, although exact compensation mechanisms other than hyperkeratosis were not identified.²¹

To find any clues for the mechanism of compensation in *Abca12*^{-/-} mice, we conducted cDNA microarray analysis. We could find that several transporters including four ATP-binding cassette (ABC) transporter family genes were up-regulated in subculture compared with primary-cultured *Abca12*^{-/-} keratinocytes. We consider these up-regulated ABC transporters as prime candidate genes to compensate for the loss of ABCA12 function. These lipid transport/metabolism-related molecules might help in lipid trafficking and/or recovery of epidermal differentiation in *Abca12*^{-/-} keratinocytes.

The recovery of skin barrier function and self-improvement of epidermal differentiation defects in mature *Abca12*^{-/-} skin gave us important clues to aid in treatment of HI patients. Infants affected with HI frequently die within the neonatal period, although the survival rate of HI newborns has increased recently with the arrival of neonatal intensive care regimes with retinoid administration.²²⁻²⁶ Our observations in mature *Abca12*^{-/-} skin further confirmed that the early neonatal period is a critical time defining the prognosis. In this context, neonatal intensive care for HI newborns in the initial neonatal period is important for their survival.

We had already tried systemic retinoid administration to pregnant mice as a fetal therapy, although neither improvement of the skin manifestations nor extension of the survival period was obtained in the *Abca12*^{-/-} newborns from the treated-mother mice.⁵ Based on the clinical efficacy of retinoids to HI patients,²²⁻²⁶ we conducted retinoid administration to the primary-cultured *Abca12*^{-/-} keratinocytes. We could not detect any recovery of differentiation defects in the primary-cultured *Abca12*^{-/-} keratinocytes treated with retinoids. These results of our therapeutic trials to fetuses in the previous report⁵ and to primary keratinocytes in this study indicated that retinoids may be ineffective for modifying the epidermal differentiation defects during the fetal period. These facts were consistent with the known effects of retinoids, which enhance proliferation and suppress differentiation of keratinocytes.^{27,28} Further, we performed a treatment trial on grafted SCID mice using systemic isotretinoin administration. Oral administration of any dose of isotretinoin (either 1 or 10 mg/kg daily, for 10 consecutive days) to the HI-skin-grafted SCID mice failed to improve the skin phenotype of grafted HI skin at all. We failed to obtain any clue to understand the reason why retinoids are only effective for HI patients from our present study.

In conclusion, we have demonstrated that disrupted epidermal keratinocyte differentiation is the pathomechanism involved in HI, and that during maturation, *Abca12*^{-/-} epidermal keratinocytes regain normal keratinocyte differentiation. This restoration of differentiation is likely to be associated with the skin phenotype improvement observed in HI survivors.

Acknowledgment

We thank Dr. James R. McMillan for proofreading this manuscript.

References

1. Akiyama M: Pathomechanisms of harlequin ichthyosis and ABCA transporters in human diseases. *Arch Dermatol* 2006, 142:914–918
2. Hovnanian A: Harlequin ichthyosis unmasked: a defect of lipid transport. *J Clin Invest* 2005, 115:1708–1710
3. Akiyama M, Sugiyama-Nakagiri Y, Sakai K, McMillan JR, Goto M, Arita K, Tsuji-Abe Y, Tabata N, Matsuoka K, Sasaki R, Sawamura D, Shimizu H: Mutations in lipid transporter ABCA12 in harlequin ichthyosis and functional recovery by corrective gene transfer. *J Clin Invest* 2005, 115:1777–1784
4. Kelsell DP, Norgett EE, Unsworth H, Teh MT, Cullup T, Mein CA, Dopping-Hepenstal PJ, Dale BA, Tadini G, Fleckman P, Stephens KG, Sybert VP, Mallory SB, North BV, Witt DR, Sprecher E, Taylor AE, Ilchshyn A, Kennedy CT, Goodyear H, Moss C, Paige D, Harper JL, Young BD, Leigh IM, Eady RA, O'Toole EA: Mutations in ABCA12 underlie the severe congenital skin disease harlequin ichthyosis. *Am J Hum Genet* 2005, 76:794–803
5. Yanagi T, Akiyama M, Nishihara H, Sakai K, Nishie W, Tanaka S, Shimizu H: Harlequin ichthyosis model mouse reveals alveolar collapse and severe fetal skin barrier defects. *Hum Mol Genet* 2008, 17:3075–3083
6. Zuo Y, Zhuang DZ, Han R, Isaac G, Tobin JJ, McKee M, Welti R, Brissette JL, Fitzgerald ML, Freeman MW: ABCA12 maintains the epidermal lipid permeability barrier by facilitating formation of ceramide linoleic esters. *J Biol Chem* 2008, 283:36624–36635
7. Akiyama M, Smith LT, Shimizu H: Expression of transglutaminase activity in developing human epidermis. *Br J Dermatol* 2000, 142:223–225
8. Raghunath M, Hennies HC, Velten F, Wiebe V, Steinert PM, Reis A, Traupe H: A novel in situ method for the detection of deficient transglutaminase activity in the skin. *Arch Dermatol Res* 1998, 290:621–627
9. Masukawa Y, Narita H, Shimizu E, Kondo N, Sugai Y, Oba T, Homma R, Ishikawa J, Takagi Y, Kitahara T, Takema Y, Kita K: Characterization of overall ceramide species in human stratum corneum. *J Lipid Res* 2008, 49:1466–1476
10. Buxman MM, Goodkin PE, Fahrenbach WH, Dimond RL: Harlequin ichthyosis with epidermal lipid abnormality. *Arch Dermatol* 1979, 115:189–193
11. Dale BA, Holbrook KA, Fleckman P, Kimball JR, Brumbaugh S, Sybert VP: Heterogeneity in harlequin ichthyosis, an inborn error of epidermal keratinization: variable morphology and structural protein expression and a defect in lamellar granules. *J Invest Dermatol* 1990, 94:6–18
12. Fleckman P, Hager B, Dale BA: Harlequin ichthyosis keratinocytes in lifted culture differentiate poorly by morphologic and biochemical criteria. *J Invest Dermatol* 1997, 109:36–38
13. Thomas AC, Tattersall D, Norgett EE, O'Toole EA, Kelsell DP: Premature terminal differentiation and a reduction in specific proteases associated with loss of ABCA12 in Harlequin ichthyosis. *Am J Pathol* 2009, 174:970–978
14. Bickenbach JR, Greer JM, Bundman DS, Rothnagel JA, Roop DR: Loricrin expression is coordinated with other epidermal proteins and the appearance of lipid lamellar granules in development. *J Invest Dermatol* 1995, 104:405–410
15. Candi E, Schmidt R, Melino G: The cornified envelope: a model of cell death in the skin. *Nat Rev Mol Cell Biol* 2005, 6:328–340
16. Denecker G, Ovaere P, Vandenebeebe P, Declercq W: Caspase-14 reveals its secrets. *J Cell Biol* 2008, 180:451–458
17. Meyer-Hoffert U, Wu Z, Schroder JM: Identification of lympho-epithelial Kazal-type inhibitor 2 in human skin as a kallikrein-related peptidase 5-specific protease inhibitor. *PLoS One* 2009, 4:e4372
18. Koch PJ, de Viragh PA, Scharer E, Bundman D, Longley MA, Bickenbach J, Kawachi Y, Suga Y, Zhou Z, Huber M, Hohl D, Kartasova T, Jarnik M, Steven AC, Roop DR: Lessons from loricrin-deficient mice: compensatory mechanisms maintaining skin barrier function in the absence of a major cornified envelope protein. *J Cell Biol* 2000, 151:389–400
19. Epp N, Furstenberger G, Muller K, de Juanes S, Leitges M, Hausser I, Thieme F, Liebisch G, Schmitz G, Krieg P: 12R-lipoxygenase deficiency disrupts epidermal barrier function. *J Cell Biol* 2007, 177:173–182
20. de Juanes S, Epp N, Latzko S, Neumann M, Furstenberger G, Hausser I, Stark HJ, Krieg P: Development of an ichthyosiform Phenotype in Alox12b-Deficient Mouse Skin Transplants. *J Invest Dermatol* 2009, 129:1429–1436
21. Kuramoto N, Takizawa T, Takizawa T, Matsuki M, Morioka H, Robinson JM, Yamanishi K: Development of ichthyosiform skin compensates for defective permeability barrier function in mice lacking transglutaminase 1. *J Clin Invest* 2002, 109:243–250
22. Prasad RS, Pejaver RK, Hassan A, Dusari S, Wooldridge MA: Management and follow-up of harlequin siblings. *Br J Dermatol* 1994, 130:650–653
23. Lawlor F, Peiris S: Harlequin fetus successfully treated with etretinate. *Br J Dermatol* 1985, 112:585–590
24. Ward PS, Jones RD: Successful treatment of a harlequin fetus. *Arch Dis Child* 1989, 64:1309–1311
25. Haftek M, Cambazard F, Dhouailly D, Reano A, Simon M, Lachaux A, Serre G, Claudy A, Schmitt D: A longitudinal study of a harlequin infant presenting clinically as non-bullous congenital ichthyosiform erythroderma. *Br J Dermatol* 1996, 135:448–453
26. Singh S, Bhura M, Maheshwari A, Kumar A, Singh CP, Pandey SS: Successful treatment of harlequin ichthyosis with acitretin. *Int J Dermatol* 2001, 40:472–473
27. Eichner R, Kahn M, Capetola RJ, Gendimenico GJ, Mezick JA: Effects of topical retinoids on cytoskeletal proteins: implications for retinoid effects on epidermal differentiation. *J Invest Dermatol* 1992, 98:154–161
28. Eichner R: Epidermal effects of retinoids: in vitro studies. *J Am Acad Dermatol* 1986, 15:789–797

Stem Cells, Tissue Engineering and Hematopoietic Elements

Blockade of Autoantibody-Initiated Tissue Damage by Using Recombinant Fab Antibody Fragments against Pathogenic Autoantigen

Gang Wang,*[†] Hideyuki Ujiie,* Akihiko Shibaki,*
Wataru Nishie,* Yasuki Tateishi,*
Kazuhiro Kikuchi,* Qiang Li,* James R. McMillan,*[†]
Hiroshi Morioka,[‡] Daisuke Sawamura,*
Hideki Nakamura,* and Hiroshi Shimizu*

From the Department of Dermatology,* Hokkaido University Graduate School of Medicine, the Creative Research Initiative Sousei,[‡] and the Faculty of Pharmaceutical Sciences,[†] Hokkaido University, Sapporo, Japan

Activation of the complement cascade via the classical pathway is required for the development of tissue injury in many autoantibody-mediated diseases. It therefore makes sense to block the pathological action of autoantibodies by preventing complement activation through inhibition of autoantibody binding to the corresponding pathogenic autoantigen using targeted Fab antibody fragments. To achieve this, we use bullous pemphigoid (BP) as an example of a typical autoimmune disease. Recombinant Fabs against the non-collagenous 16th-A domain of type XVII collagen, the main pathogenic epitope for autoantibodies in BP, were generated from antibody repertoires of BP patients by phage display. Two Fabs, Fab-B4 and Fab-19, showed marked ability to inhibit the binding of BP autoantibodies and subsequent complement activation *in vitro*. In the *in vivo* experiments using type XVII collagen humanized BP model mice, these Fabs protected mice against BP autoantibody-induced blistering disease. Thus, the blocking of pathogenic epitopes using engineered Fabs appears to demonstrate efficacy and may lead to disease-specific treatments for antibody-mediated autoimmune diseases. (Am J Pathol 2010, 176:914–925; DOI: 10.2353/ajpath.2010.090744)

Autoimmune diseases are a major cause of morbidity and mortality in humans, affecting approximately 5% of the general population.¹ In recent years, significant ad-

vances have been made in our understanding of autoimmune disease pathomechanisms, especially the roles of autoantibodies, complement system, and autoreactive T cells. For many autoimmune diseases such as systemic lupus erythematosus, rheumatoid arthritis, anti-phospholipid syndrome (APS), and bullous pemphigoid (BP), complement activation is increasingly recognized as critical to tissue injury.^{2–6} Studies of APS and BP, for example, showed that the classical pathway of complement activation is required for the development of tissue injury, although alternative pathways may also be involved.^{4,7–9}

BP is the most common autoimmune blistering skin disease. Autoantibodies against collagen XVII (COL17) bind to dermal–epidermal junction (DEJ) components and activate the complement system that mediates a series of inflammatory events including dermal mast cell degranulation and generation of eosinophil-rich infiltrates, resulting in skin blister formation.^{10–12} APS is a condition characterized by recurrent miscarriage and thrombosis in the presence of anti-phospholipid autoantibodies, and a therapy has been proven effective to prevent the fetal loss by using heparin to inhibit anti-phospholipid antibody-induced complement activation.^{7,13,14} In both BP and APS, F(ab')₂ fragments from the pathogenic autoantibodies, which lack the Fc portion necessary to activate the complement pathway, fail to initiate the disease.^{4,7} This suggests that preventing complement activation by blocking the binding of autoantibodies to the corresponding antigens can be a viable novel therapeutic strategy for treating these diseases.

Supported by a grant-in-aid from the Program for Promotion of Fundamental Studies in Health Sciences of the National Institute of Biomedical Innovation (NIBIO; to H.S.).

G.W. and H.U. contributed equally to this work. A.S. and H.S. contributed equally to the direction of this study.

Accepted for publication October 7, 2009.

Supplemental material for this article can be found on <http://ajp.amjpathol.org>.

Address reprint requests to Dr. Akihiko Shibaki or Dr. Hiroshi Shimizu, Department of Dermatology, Hokkaido University Graduate School of Medicine, N15 W7, Sapporo, 060-8638 Japan. E-mail: ashibaki@med.hokudai.ac.jp or shimizu@med.hokudai.ac.jp.

Table 1. PCR Primers for the Amplification of Human Antibody Gene Repertoires

Primers for κ	
HK5	5'-GAMATY <u>GAGCTCAC</u> SCAGTCTCCA-3' (Sac I)
HK3	5'-GCGCCG <u>TCTAGA</u> ACTAACACTCTCCCTGTTGAAGCTCTTTGTGACGGGCAAG-3' (Xba I)
Primers for λ	
HL5	5'-CASTYTGAGCTCACKCARCCGCCCTC-3' (Sac I)
HL3	5'-GAGGGAT <u>TCTAGA</u> ATTATGAACATTCTGTAGG-3' (Xba I)
Primers for Fd	
H135	5'-CAGGTGCAGCTGGTGSAGTCTGG-3'
H2	5'-CAGGTCAACTTGAAGGAGTCTGG-3'
H4	5'-CAGGTGCAGCTGCAGGAGTCCGG-3'
VH5	5'-CAGGTGCAGCTC <u>GAG</u> SAGTCTGG-3' (Xho I)
HG3	5'-GCATGT <u>ACTAGT</u> TTTGTGCAAGA-3' (Spe I)

To allow for sequence variability, representative choices of wobble nucleotides were included in the primers (M = A/C, K = G/T, R = A/G, S = C/G, Y = C/T). Fd fragments of human IgG were amplified in a two-step procedure. First, antisense primers H135, H2, and H4 were combined with HG3 for the amplification of heavy chain genes from human VH1-VH5 families and the Spe I site was introduced. In the second step, antisense primer VH5 was combined with HG3 to reamplify the heavy chain genes and introduce the Xho I site. Underlined sequences are restriction sites for the enzymes indicated in parenthesis.

The purpose of this study is to provide a proof of concept for this new strategy of treating antibody-mediated autoimmune disorders by using recombinant Fabs to block complement activation induced by pathogenic autoantibodies. Toward this end, we use BP as an example of a typical autoimmune disease. Our group has recently established a BP mouse model using a newly constructed COL17 humanized mouse.³ Here we report our success in developing Fabs against the noncollagenous 16th-A domain (NC16A) of COL17, the main pathogenic epitope of BP autoantibodies,¹⁵ for the blockade of autoantibody-initiated BP disease.

Materials and Methods

Construction of Phage Antibody Libraries

We constructed two individual Fab phage libraries from mononuclear cells isolated from two patients with active BP. The diagnosis of BP was made by the typical clinical and histological manifestations as well as by laboratory data including anti-COL17 ELISA and indirect immunofluorescence (IIF). Phagemid expression vector p3MH, a gift from Dr. Yan Wang (Central Lab of Navy General Hospital, Beijing, China), was derived from pCOMB3H (Scripps Research Institute, La Jolla, CA) by adding 9E10/c-myc epitope for detection and a hexahistidine tag for column purification at the 3' end of Fd.¹⁶ Using previously described methods and a set of PCR primers (Table 1),¹⁷⁻¹⁹ antibody genes were amplified by RT-PCR from approximately 1×10^8 mononuclear cells isolated from 50 ml of peripheral blood from each patient. The phage antibody libraries were constructed by randomly combining the genes coding Fd fragments of IgG heavy chains with IgG light chain genes of either lambda or kappa DNA in equal amounts (see Supplemental Figure S1 at <http://ajp.amjpathol.org>). The phagemid libraries were electroporated into *E. coli* XL1-Blue strain (Stratagene, La Jolla, CA), and the phage display of the libraries was performed as described elsewhere.^{17,20} Before amplification, the resulting libraries were examined for the coexpression of heavy and light chains by enzyme digestion and for the diversity by fingerprinting of antibody genes (Fd and light chain) of 24 randomly selected single colo-

nies.^{20,21} The amplified recombinant phages were purified from culture supernatants by polyethylene glycol precipitation and resuspended in PBS, pH 7.4, containing 1% bovine serum albumin (BSA) and 10% glycerol.

Isolation of Phage Antibodies against NC16A Domain of Human COL17

Recombinant fusion peptide of the human COL17 NC16A domain (rhNC16A) with glutathione S-transferase (GST) was synthesized as reported previously.³ Library panning was performed routinely.²⁰⁻²² Briefly, a freshly amplified phage library (approximately 1×10^{12} phages) was incubated for 2 hours at 37°C in immuno-tubes (Nunc, Roskilde, Denmark) coated with 50 μ g/ml rhNC16A in 50 mmol/L NaHCO₃ pH 9.6. After washing of the tube with 0.05% (v/v) Tween-20 in PBS, adherent phages were eluted with 0.1 mol/L triethylamine (Sigma-Aldrich, Inc., St. Louis, MO). After neutralization with 1 mol/L Tris, pH 7.4, eluted phages were used to infect a fresh culture of XL1-Blue *E. coli*, which was amplified overnight as previously described.²⁰ Phages were harvested from culture supernatants and then repanned against rhNC16A for three subsequent rounds as described for the original library. Individual single ampicillin-resistant colonies resulting from infection of *E. coli* XL1-Blue with the eluted phage from the fourth panning round were isolated, and the binding to rhNC16A was confirmed by ELISA using HRP-conjugated anti-M13 mAb (Amersham Biosciences UK Ltd., Little Chalfont, Buckinghamshire, UK) as the developing reagent. The specific binders were screened by gene fingerprinting and sequencing to identify different clones. The variable region sequences of the separate selected clones were analyzed for homology to known human V, D, and J genes using the V BASE database (<http://vbase.mrc-cpe.cam.ac.uk/>).

Production, Purification, and Characterization of Soluble Fab

Fab Production and Purification

Plasmid DNA of the distinct selected clones was prepared, digested by *NheI* (New England BioLabs,

Ipswich, MA) to remove the gene III fragment, self ligated, and transformed into *E. coli* XL1-Blue. Clones were grown in LB containing 100 $\mu\text{g/ml}$ ampicillin, and Fab expression was induced using 1 mmol/L isopropyl β -D-thiogalactopyranoside (IPTG, Sigma) in culture grown at 30°C overnight. Cells were pelleted by centrifugation, and the supernatant containing soluble Fab was taken for analysis.

Large-scale production of Fabs was achieved by growing Fab-express clones in *E. coli* XL1-Blue in 1 L of LB (plus 100 $\mu\text{g/ml}$ ampicillin). Protein production was then induced with 1 mmol/L IPTG by culturing overnight at 30°C at 240 rpm. The culture supernatant was harvested by centrifugation. Fab purification was performed using HisTrap FF crude column (GE Healthcare Bio-Sciences AB, Uppsala, Sweden) according to the manufacturer's instructions. The purified Fabs were dialyzed against PBS and concentrated by Amicon ultrafiltration (Millipore, Lexington, MA) and were then characterized by SDS-PAGE and Western blotting. For animal experiments, the concentration of endotoxin in the purified Fabs was detected with the limulus amoebocyte lysate test using the QCL-1000 kit (Cambrex Bio Science Walkersville, Inc., Walkersville, MD), and endotoxin removal was performed by using Detoxi-Gel AffinityPak column (Pierce, Rockford, IL), where necessary.

ELISA

The binding activity and specificity of Fabs was confirmed by ELISA assay. ELISA plate wells were coated with 5 $\mu\text{g/ml}$ rhNC16A in 50 mmol/L NaHCO_3 pH 9.6. Recombinant mouse NC16A (rmNC16A), GST, and BSA were used as negative control antigens at similar concentrations. Supernatant containing Fabs or appropriately diluted purified Fabs was incubated on ELISA plates. After washing, plates were developed with HRP-conjugated mAbs to human lambda light chain (Kirkegaard & Perry Laboratories, Gaithersburg, MD) or kappa light chain (Bethyl Laboratories, Inc., Montgomery, TX) and o-phenylenediamine substrate (Wako, Osaka, Japan). Absorbance was read at 492 nm.

Western Blotting

Western blotting was performed as previously described. Briefly, recombinant proteins were electrophoresed on SDS-PAGE and electrotransferred onto nitrocellulose membrane. The blots were blocked with 5% milk in TBS/T and incubated for 1 hour with the diluted Fabs at room temperature. After washing, the blots were incubated with HRP-conjugated mAbs to human lambda light chain or kappa light chain. The bound antibodies were detected by the Phototope Western Detection Systems (Cell Signaling Technology, Inc., Danvers, MA).

Epitope Mapping

Epitope mapping studies were performed using the standard Western blotting protocol described above. The

NC16A domain of human COL17 was divided into subregions as described by Giudice et al.^{15,23} The expression vectors NC16A1, NC16A2, NC16A2.5, and NC16A3, which respectively correspond to amino acid segments 490 to 506, 507 to 520, 514 to 532, and 521 to 534, were gifts from Dr. George J Giudice (Medical College of Wisconsin, Milwaukee). Affinity purified products of recombinant human NC16A and its subregions were electrophoresed and electrotransferred to nitrocellulose membrane. The membranes were then probed with Fabs and allowed to react with HRP-conjugated secondary mAbs to human lambda light chain or kappa light chain.

Immunogold Electron Microscopy

Normal human skin samples were processed for postembedding immunoelectron microscopy as previously described.^{24,25} Briefly, cryofixed cryosubstituted samples were embedded in Lowicryl K11M resin and polymerized at -60°C under UV light. Selected blocks were used to produce ultrathin sections that were incubated with Fabs (80 $\mu\text{g/ml}$), diluted in PBS-based buffer, and washed four times (five minutes each). Further incubations were performed using rabbit anti-c-myc tag antibody (Santa Cruz Biotechnology, Santa Cruz, CA) followed by four washes and further incubation with 5-nm gold-conjugated antibody for immunogold labeling (Biocell, Cardiff, UK) diluted 1 in 200 in TBS buffer. Other primary anti-COL17 antibodies included for comparison were HD4 233, 1D1, and 1A8C, each of which recognizes different domains of human COL17 (extracellular domain close to the C-terminal, mid portion, and cytoplasmic domains, respectively).²⁶ Sections were viewed under a Hitachi H-7100 transmission electron microscope (Hitachi, Tokyo, Japan) at 80 KV.

Immunofluorescence

Five- μm cryosections of OCT-embedded skin were cut and placed onto microscope slides and subjected to IF studies. IIF using Fabs was performed on the skin samples from human or COL17 humanized mice using a standard protocol. FITC conjugated secondary antibodies against human lambda light chain (DakoCytomation, Glostrup, Denmark), kappa light chain (Invitrogen Corp., Carlsbad, CA), or c-myc tag (Santa Cruz Biotechnology) were used as detection reagents.

Surface Plasmon Resonance Analysis

Affinity of the generated Fabs was determined by BiAcore assay. The on and off rate constants (k_{on} and k_{off}) for binding of the Fabs to rhNC16A were determined by a BiAcore 2000 instrument (Biacore AB, Uppsala, Sweden). For analysis of the interaction kinetics, Fabs in various concentrations (100, 80, 60, 50, and 40 nmol/L) were injected over the immobilized antigen at a flow rate of 20 $\mu\text{l/min}$ using HBS-EP buffer (Biacore AB). The association and dissociation phase data were fitted simultaneously to a 1:1 Langmuir global model by using the

BIAevaluation software. The affinities (dissociation constant, K_D) were calculated from the ratio of the rate constants of association and disassociation (k_{on}/k_{off}).

Functional Analysis of Fabs in Vitro

Preparation of BP Autoantibodies

BP autoantibodies were purified from either pooled sera from 20 patients or were included as separate serum samples from three patients with active BP. Briefly, the total IgG fraction from BP sera was prepared by affinity chromatography using HiTrap Protein G HP column (Amersham Biosciences UK Limited). Then, BP autoantibodies against the COL17 NC16A peptide were affinity purified from the IgG fraction using HiTrap NHS-activated HP column (Amersham Biosciences UK Ltd.) precoated with rhNC16A according to the manufacturer's instructions.³ The NC16A affinity purified BP autoantibodies were dialyzed against PBS and concentrated by Amicon ultrafiltration (Millipore). These NC16A affinity purified BP autoantibodies were designated as BP antibodies (BPABs), and used for *in vitro* inhibition experiments.

For the *in vivo* experiments using whole BP-IgG fractions as the pathogenic autoantibodies, serum samples were collected from another 10 BP patients and total IgG fraction was prepared using HiTrap NHS-activated HP column. This was designated as BP-IgG. Binding activity with different autoantigens was tested by ELISA and Western blotting. The BP-IgG from all ten of the serum samples bound to human COL 17, and the BP-IgG from seven of the ten serum samples also reacted with BP230. The binding of the BP-IgG with the subdomains of NC16A (NC16A-1, -2, -2.5, -3, as described by Giudice et al¹⁵) was further studied. All ten of the serum samples bound to NC16A-2 and NC16A-2.5. In addition, two of the ten serum samples also bound to NC16A-1 or -3. When the pooled IgG from these ten patients was first incubated with the NC16A domain of COL17 overnight at 4°C, the reaction with the NC16A domain was markedly reduced, whereas binding to the full length COL17 was unchanged by Western blotting. This indicates that the BP-IgG recognize numerous epitopes on both COL17 and BP230 antigens, and that there exist autoantibodies recognizing different epitopes both within and outside of the COL17 NC16A domain.

Inhibition ELISA

To check the competition effect of Fabs on the binding of BPABs to rhNC16A, an inhibition ELISA was performed by incubating purified BPABs (8 $\mu\text{g}/\text{ml}$) with 0 to 32 $\mu\text{g}/\text{ml}$ Fabs on rhNC16A ELISA plates. To detect the IgG autoantibodies, the plates were developed with HRP-conjugated polyclonal antibody to human IgG (DakoCytomation) and o-phenylenediamine substrate. Absorbance was read at 492 nm. The reduced reaction of BPABs with rhNC16A was expressed as an inhibition rate, which was calculated according to the following formula: inhibition rate % = $(A_{492b} - A_{492f})/A_{492b} \times 100$, where A_{492b} is

the reaction with BPABs only and A_{492f} is the reaction competed with Fab at a given concentration.

Inhibition ELISA between phage antibodies (Phabs) and Fabs from the isolated clones was performed to determine whether the Fabs against different epitopes mutually cross-inhibit binding by steric hindrance. Individual Phabs were incubated with rhNC16A on ELISA plates. The reaction was challenged with Fabs from different clones at various concentrations. After washing, the remaining binding of the Phabs to rhNC16A was developed with the HRP-conjugated anti-M13 antibody and o-phenylenediamine substrate.

Inhibition IF

Inhibition IF was assessed to check the competition of Fabs to the binding of BPABs by incubating purified BPABs (10 $\mu\text{g}/\text{ml}$) with 0 to 40 $\mu\text{g}/\text{ml}$ Fabs on human skin sections. FITC-conjugated anti-human IgG (DakoCytomation) was the detection reagent. The inhibition IF was also performed by sequential incubation with BPABs on human skin sections, which was followed by Fabs with a 30-minute interval. The effects of Fab inhibition on the binding of autoantibodies from patients with linear IgA bullous dermatosis and anti-p200 pemphigoid were also observed.

In Vitro Inhibition of BPAB-Induced Complement Activation

BPAB-induced complement activation in human skin samples and the inhibitory effects of anti-COL17 NC16A Fabs were observed by IF as described by Nelson et al with minor modifications.⁹ Cryosections of normal human skin were incubated with BPABs (10 $\mu\text{g}/\text{ml}$), anti-COL17 NC16A Fabs (10 to 40 $\mu\text{g}/\text{ml}$), or BPABs plus anti-COL17 NC16A Fabs for one hour at 37°C. Freshly prepared normal human serum was then added as a complete complement source. One hour after incubation, *in situ* deposition of human C1q and C3 at the DEJ was detected with FITC-conjugated mAbs to human C1q and human C3 (DakoCytomation), respectively.

Effects of Fabs on BP Mouse Model in Vivo

All mouse procedures were approved by the Institutional Animal Care and Use Committee of Hokkaido University, and the experimental mice were housed in a specific pathogen-free animal facility. The BP model mice were produced by injecting BP autoantibodies, either NC16A affinity purified BPABs (50 $\mu\text{g}/\text{g}$ body weight) or whole BP-IgG (1 mg/g body weight) prepared from BP patients, into the COL17 humanized neonatal mice, as previously reported.³ At 48 hours after the injection, the mice developed human BP-like clinical and histological characteristics with serum autoantibody titers ranging from 1:80 to 1:640 in IIF and a mean BP180 antibody index value of 55.7 ± 21.1 by ELISA measurement, which is similar to the autoantibody level usually found in the sera of active BP patients. To observe the effects of the generated

anti-COL17 NC16A Fabs on the COL17 humanized mice and on the BPAB-induced disease, we divided the neonatal mice into different groups. We first injected Fabs from the three individual clones to test whether the recombinant Fabs themselves are pathogenic in COL17 humanized mice. The Fab doses were 30 to 90 $\mu\text{g/g}$ body weight (30 $\mu\text{g/g}$ body weight is roughly an equimolar dose compared with 50 $\mu\text{g/g}$ body weight of IgG-BPABs). To sequentially monitor the serum Fab levels after injection, 60 $\mu\text{g/g}$ body weight of Fab-B4 was injected into the neonatal mice and blood samples were collected by sacrificing mice at 6, 24, 48, and 72 hours. The Fab concentration was quantified using a sandwich ELISA technique with two mAbs. To capture Fabs in the samples, rabbit anti-*c-myc* mAb (Santa Cruz Biotechnology) was coated onto ELISA plates (20 $\mu\text{g/ml}$ in PBS overnight at 4°C). After blocking with 3% BSA for one hour at 37°C, individual serum samples were diluted with 1% BSA in PBS buffer (1:10) and incubated for 1 hour at 37°C. Purified Fab was used as a standard at concentrations ranging between 0.1 $\mu\text{g/ml}$ and 50 $\mu\text{g/ml}$. The plate was then incubated with HRP-conjugated mouse anti-human lambda light-chain mAb to detect the reaction. The concentrations of Fabs in the samples were calculated from the standard curve for each plate.

The effects of Fabs on the BP autoantibody-induced mouse model were observed by injecting Fabs either from individual clones or from various combinations of the clones. The injection of antibodies into mice was performed as described previously, with minor modifications.³ Briefly, each mouse received a single intraperitoneal injection of different antibodies according to group. At 48 hours after injection, the extent of skin disease was judged, including distinct Nikolsky sign. The animals were then sacrificed, and skin samples were studied by light microscopy and direct immunofluorescence microscopy using FITC conjugated antibodies against human lambda light chain (DakoCytomation), *c-myc* tag (Santa Cruz Biotechnology), human IgG (Jackson, West Grove, PA), and mouse complement C3 (Cappel, ICN Pharmaceuticals, Inc., Aurora, OH). The quantification of mast cells (MCs) and MC degranulation was performed as described by Nelson et al, and the results were expressed as a percentage of degranulated MCs (number of degranulated MCs per total number of MCs in 5 random fields \times 100%).⁹

Blood was collected, and the serum sample was prepared and used for ELISA to determine the titers of circulating BPABs or Fabs. The level of BPABs in the serum samples of experimental mice was tested using an anti-COL17 ELISA kit according to the manufacturer's instructions (MBL, Nagoya, Japan). Absorbance was read at 450 nm. The index value was defined by the following formula: index = (A450 of tested serum - A450 of negative control)/(A450 of positive control - A450 of negative control) \times 100. The concentration of the recombinant Fabs in serum samples obtained from the experimental mice was quantified using the sandwich ELISA technique described above.

Statistical Analysis and Ethical Considerations

Differences in the ELISA inhibition results among various groups were examined for statistical significance using the analysis of variance with Fisher PLSD test. For the analysis of MC degranulation among various groups of Fab treatments, we determined statistical significance using multiple tests including the Student *t* test and one way analysis of variance. *P* values less than 0.05 were considered significant.

This study was approved by the Institutional Review Board of Hokkaido University, and fully informed consent from all patients was obtained for use of human material.

Results

Isolation of Anti-COL17 NC16A Antibodies from Phage Antibody Libraries

Two individual Fab phage libraries containing 8×10^7 clones and 4×10^7 clones, respectively, were successfully constructed by combining light chain genes and heavy chain genes amplified from antibody repertoires of two BP patients (library 1 from patient 1; library 2 from

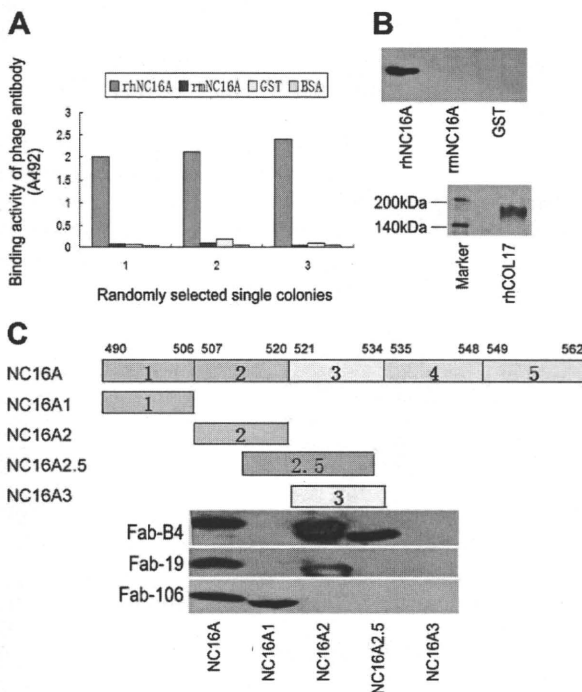


Figure 1. Isolation of specific binders against the NC16A domain of human type XVII collagen from phage antibody library. **A:** Randomly selected single colonies from the fourth panning round of the libraries show positive reaction with recombinant human NC16A (rhNC16A) but no reaction with recombinant mouse NC16A (rmNC16A), GST, or BSA in ELISA. **B:** Western blotting of soluble Fabs shows staining of only the rhNC16A domain and full-length human COL17, whereas rmNC16A and GST are negative. The representative results using Fab-B4 are shown. **C:** Epitope mapping of the generated Fabs with rhNC16A and its subdomains are shown. Fab-B4 binds to rhNC16A, NC16A2, and NC16A2.5 but does not react with NC16A1 and NC16A3, indicating that the binding epitope is located within an overlapping region within subdomain 2 and 2.5 (amino acids 514 to 520). The Fab-106 and Fab-19 epitopes are located in subdomain 1 (NC16A1, amino acids 490 to 506) and subdomain 2 (NC16A2, amino acids 507 to 520), respectively.

Table 2. Heavy and Light Chain Genes of Isolated Fabs

Fab clone	VH family	Amino acid sequences of VH			VL family	Amino acid sequences of VL		
		CDR1	CDR2	CDR3		CDR1	CDR2	CDR3
B4	VH1	NYAFSW	GIIPMSGEGHKAQKFQG	PSRSNYAGGMDV	VA1	SGSSSNIGRHVYV	TNYRRPS	ASWDDSL
B12	VH3	SYSMN	SISSSSYIYADSVKG	IDSSWYEGWFDP	VA1	SGSTSNIGSNTVN	SNNQRLS	GTWDDSLN
B21	VH3	SYVLS	LLVVMLEADTTQTPEG	GNNWYQTFDF	VA1	GAAPTSGQVMYTW	GNSNRPS	QSYDSSL
F32	VH3	SYAMH	VISYDGSNKYADSVKG	ALRGYSYGT	Vk1	RASQSISSYLN	AASSLQS	QSYSLF
19	VH3	NYGMH	VISYDGSKKYADSVKG	GFYDWTYYDY	VA1	TGSSSNIGAGYDVH	ANSNRPS	QSYDSSLT
106	VH3	DSAIH	RVRSKTNNYATDYAVSVKGR	HGESRSWYVSGYWFDP	VA1	SGSSSNIGNNYVS	DNNKRPS	GTWDDSL

Six unique antibody clones against the NC16A domain of human COL17 were identified by sequencing the heavy and light chain variable regions. Of these, clones B4, B12, B21, and F32 were isolated from library 1, whereas clones 19 and 106 were isolated from library 2. The deduced amino acids sequences of the complementary determining regions (CDRs) are shown.

patient 2). Phabs were selected by panning against rhNC16A immobilized on immune tubes. ELISA of the Phabs revealed specific positive reactions with rhNC16A in 40 of 96 and 32 of 80 colonies isolated from the two libraries, respectively (Figure 1A). By BstNI fingerprinting and sequencing of variable regions of heavy chain (VH) and light chain (VL) genes, nine unique antibody clones against rhNC16A were identified and were allowed to express the soluble Fab fragments.

Expression and Characterization of Fabs

Soluble Fab fragments of the nine antibody clones were successfully expressed by removing the gene III fragment of the phagemid vector. Four of the soluble Fabs from library 1 (Fab-B4, Fab-B12, Fab-B21, Fab-F32) and two from library 2 (Fab-19, Fab-106) were highly specific to rhNC16A in ELISA (data not shown) and Western blot analysis (Figure 1B, representative Western blot result). The other three clones, however, could not be detected as soluble fragments, probably because of their low affinity. The VH and VL genes of the six positive Fab clones are summarized in Table 2.

By epitope mapping, the binding site of the Fabs with rhNC16A and its subdomains was obtained. All four of the Fabs from library 1 showed the same reactive pattern. They bound to rhNC16A and subdomains 2 and 2.5 but failed to react with subdomains 1 and 3, indicating that their binding epitope was within the overlapping region (amino acids 514 to 520) of subdomains 2 and 2.5. The two Fabs from library 2 bound to different subdomains: Fab-106 reacted only with subdomain 1 (amino acids 490 to 506) and Fab-19 reacted only with subdomain 2 (amino acids 507 to 520). This indicates that they bound to different epitopes on COL17 NC16A. The representative blot results are shown in Figure 1C. These data demonstrate the successful isolation of anti-COL17 NC16A Fabs from patients with BP.

We chose Fabs (Fab-B4, Fab-19, and Fab-106) that had been raised against different epitopes of COL17 NC16A for further experiments. All of the light chains of these three clones are from human lambda light chain family. Large-scale production was performed, and a yield of approximately 1 to 3 mg of Fab product was obtained from each 1 L culture after column purification. Figure 2A shows the SDS-PAGE identification of the purified Fab in reduced and nonreduced form.

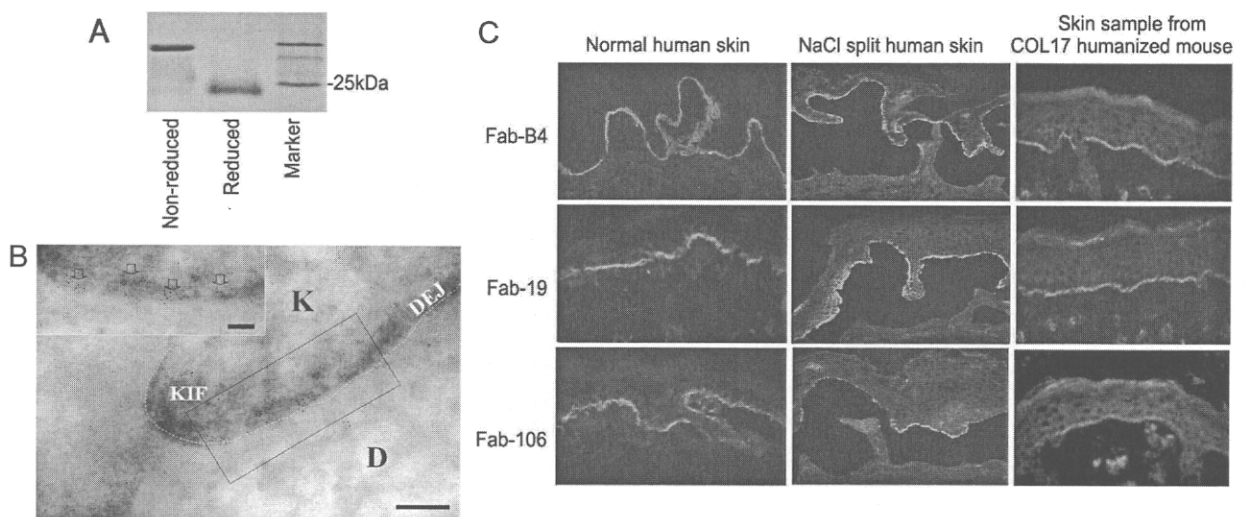


Figure 2. Production and characterization of Fabs. **A:** A purified soluble Fab in both reduced and nonreduced states is shown by Coomassie blue staining after SDS-PAGE. **B:** Immunogold labeling of normal human skin by Fabs shows 5-nm immunogold deposits restricted to immediately beneath hemidesmosomes, close to the keratinocyte plasma membrane (arrows, bar = 100 nm). The representative results using Fab-B4 are shown. (K: keratinocyte; D: dermis; KIF: keratin intermediate filaments; DEJ: dermal-epidermal junction). **C:** Immunofluorescence studies on normal human skin and skin sections from COL17 humanized mice show positive staining of the selected Fabs at the DEJ, and positive staining is also noted on the roof of NaCl split skin samples.

Table 3. Affinity of Anti-COL17 NC16A Fabs Measured by BIAcore System

Fab	k_{on} (1/Ms)	k_{off} (1/s)	K_D (M)
Fab-B4	2.83×10^5	1.10×10^{-3}	3.89×10^{-9}
Fab-19	1.14×10^5	6.26×10^{-3}	5.48×10^{-8}
Fab-106	5.52×10^5	8.08×10^{-2}	1.46×10^{-7}

Kinetic parameters k_{on} and k_{off} were measured by BIAcore system, and K_D was calculated as k_{on}/k_{off} . From the three Fabs, Fab-B4 has the highest affinity.

Immunogold electron microscopy showed that 5-nm immunogold particles were restricted to immediately beneath hemidesmosomes, below the keratinocyte plasma membrane (Figure 2B). Mean measurements of immunogold deposits demonstrated that their epitopes were about 1 to 2 nm (mean 1.77 nm \pm SD, $n > 200$) beneath the plasma membrane and located between the epitopes of 1A8C, a cytoplasmic plaque associated COL17 antibody and 233 (an extracellular COL17 antibody), as described by Nonaka et al.²⁶ No difference in distribution of the immunogold deposits was found between the three Fabs.

In the IIF experiments, as we expected, all three Fabs showed linear deposition at the DEJ and positive staining

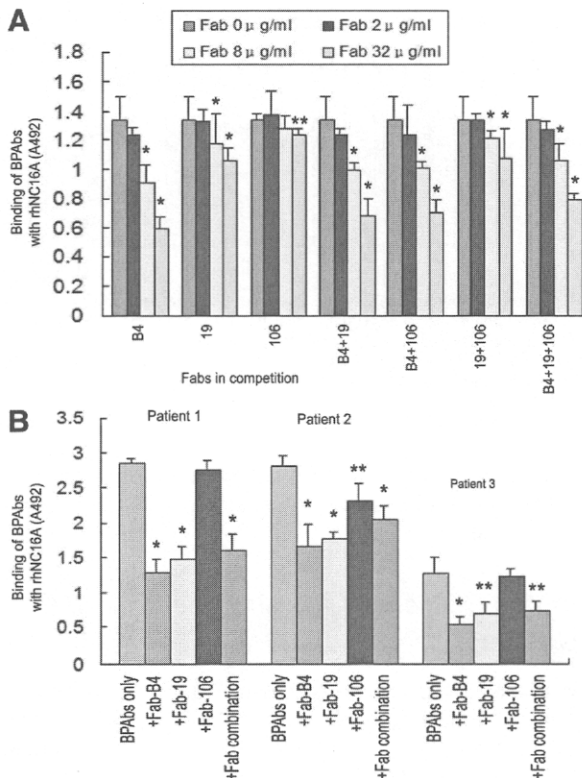


Figure 3. Inhibition ELISA assay. **A:** The effects of competition with Fab-B4, Fab-19, and various combinations inhibit the binding of autoantibodies (BPABs, 8 μ g/ml) from pooled sera of patients with bullous pemphigoid (BP) to rhNC16A in a dose-dependent manner (0 to 32 μ g/ml), whereas Fab-106 inhibits BPAB binding only moderately. * $P < 0.01$, ** $P < 0.05$, versus the original binding of BPABs. **B:** Fabs (32 μ g/ml) inhibit the binding of BPABs from three BP patients. * $P < 0.01$, ** $P < 0.05$, versus the original binding of BPABs.

was noted along the roof of the NaCl split skin samples, consistent with COL17 staining (Figure 2C).

Kinetic analysis using the BIAcore system demonstrated affinity levels of Fab-B4, Fab-19, and Fab-106, as summarized in Table 3. Among these Fabs, Fab-B4 showed the highest affinity value and Fab-106 showed the lowest.

Functional Analysis of Fabs in Vitro

To determine whether the Fabs generated against COL17 NC16A were able to function in competitive binding to inhibit the emergence of an autoantibody-mediated BP phenotype, we initially performed a series of *in vitro* experiments to evaluate their ability to block BP autoantibody binding to COL17. Figure 3A shows that the rhNC16A binding activities of BPABs, which were affinity purified using recombinant COL17 NC16A peptide from the pooled sera from 20 BP patients, were reduced markedly and significantly by Fab-B4 and Fab-19, but only marginally by Fab-106, in a dose-dependent manner (0 to 32 μ g/ml). Fab-B4 and 19 suppressed the binding of BPABs most efficiently at a concentration of 32 μ g/ml, with the highest inhibition rates of 52.4% and 50.8%, respectively. Combinations of two or three Fabs failed to increase this inhibition efficacy. When tested with BPABs isolated from individual BP patients, Fabs showed similar competitive effects (Figure 3B).

IIF studies show competitive blocking of Fabs with BPABs on skin sections. Figure 4 shows positive IgG

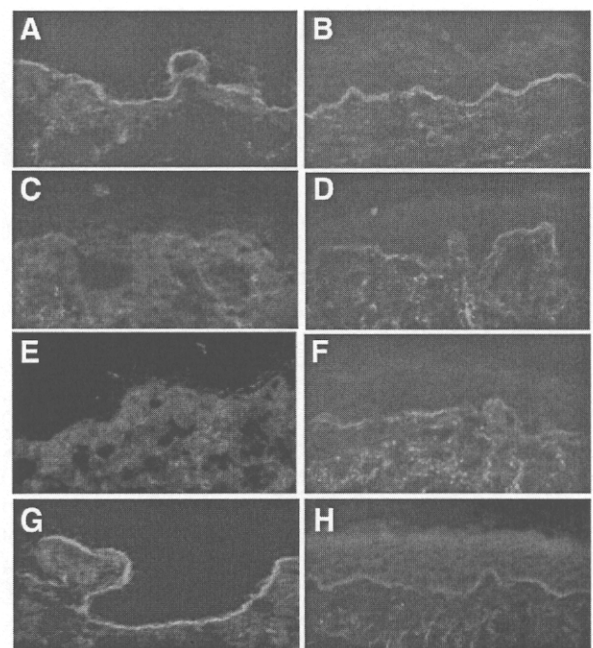


Figure 4. Inhibition immunofluorescence. **A and B:** Positive IgG staining of the NC16A affinity purified BPABs (10 μ g/ml) at the DEJ in human skin. **C and E:** IgG BPABs staining is blocked by coincubation with either Fab-B4 or Fab-19 at a concentration of 20 μ g/ml. **G:** Fab-106 (20 μ g/ml) fails to significantly inhibit the binding of BPABs. When BPABs are allowed to bind to skin sections first and Fabs are added 30 minutes later, the IF staining of BPAB binding is also markedly reduced by Fab-B4 (**D**) or Fab-19 (**F**) but not by Fab-106 (**H**).

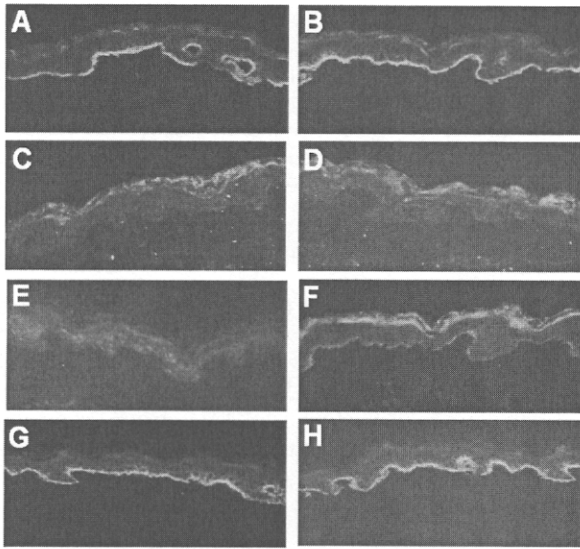


Figure 5. BPAb-induced complement activation and the inhibitory effects of Fabs. NC16A affinity purified BPAbs (10 $\mu\text{g/ml}$) induced activation of human C1q and C3 is shown at the DEJ in cryosections of human skin (A and B). When Fabs are coadministered with BPAbs at the same concentration, Fab-B4 completely blocks C1q and C3 activation (C and D), whereas Fab-19 effectively blocks the activation of C1q (E) and markedly reduces the activation of C3 (F). Fab-106 shows no inhibition of either C1q or C3 activation (G and H).

BPABs staining (10 $\mu\text{g/ml}$) at the DEJ in human skin (Figure 4A), which was blocked by coincubation with either Fab-B4 or Fab-19 at a concentration of 20 $\mu\text{g/ml}$ (Figure 4, C and E). Fab-106 failed to significantly inhibit the binding of BPABs (Figure 4G). When BPABs were allowed to bind to skin sections first and Fabs were added 30 minutes later, the IF staining of BPAB binding was also markedly reduced although not completely inhibited (Figure 4, B, D, F, and H). Competitive IF using Fabs and individual patient BPABs showed that Fab-B4 and Fab-19 were able to block the binding of autoantibodies from three individual BP patients, whereas none of the Fabs inhibited the binding of IgA autoantibodies from patients with linear IgA bullous dermatosis or IgG autoantibodies from patients with anti-p200 pemphigoid (data not shown).

In vitro inhibition of complement activation by recombinant Fabs was studied by immunofluorescence. *In situ* deposition of BPAB-activated C1q (Figure 5A) and C3 (Figure 5B) was found at the DEJ in human skin. Complement deposition was reduced or completely blocked by Fab-B4 (Figure 5, C and D) or Fab-19 (Figure 5, E and F), whereas it was unchanged by Fab-106 treatment (Figure 5, G and H). Fabs against COL17 NC16A did not activate complement at concentrations up to 100 $\mu\text{g/ml}$.

We also tested the effect of competition between recombinant anti-COL17 NC16A Fabs. Using an inhibition ELISA, Fabs from the three clones inhibited the binding of Phabs from their own clone as we might have expected. Interestingly, Fab-B4 and Fab-19 cross-inhibited each other while Fab-106 failed to inhibit the other two (Figure 6, A–C). These data indicate that Fab-B4 and Fab-19 specifically recognize distinct but close or overlapping

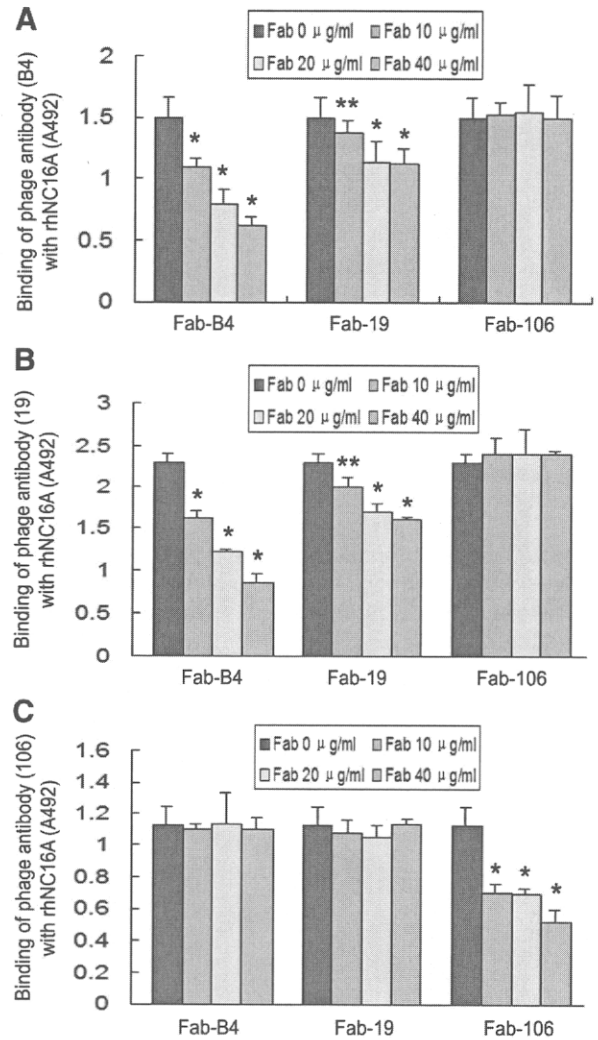


Figure 6. Inhibition ELISA for the three recombinant antibody clones using Fabs and phage antibodies (Phabs). Fab-B4 and Fab-19 inhibited the binding of both Phab-B4 and Phab-19 (A and B), whereas Fab-106 inhibited Phab-106 only (C). This indicates that the antibody clones B4 and 19 are mutually cross-inhibiting. * $P < 0.01$, ** $P < 0.05$, versus the original binding of respective Phabs.

epitopes and are able to block the binding of BP antibodies in nearby epitopes, most likely by direct steric hindrance.

In Vivo Blockade of Autoantibody-Induced BP Disease

We first proved that recombinant Fabs were not pathogenic to COL17 humanized mice after injection with 30 to 90 $\mu\text{g/g}$ body weight of Fab-B4, -19, or -106 into neonatal mice. Neither clinical signs, including erythema and Nikolsky sign, nor any histopathological manifestations of BP were found in the treated mice. Direct immunofluorescence studies demonstrated clear deposition of the recombinant Fab fragments at the DEJ. Subsequent deposition of mouse C3 was not detected (Figure 7A).